2007

Predicting the dispersion and viability of maize pollen

Brian J. Viner
Iowa State University

Predicting the dispersion and viability of maize pollen

by

Brian J. Viner

A thesis submitted to the graduate faculty

in partial fulfillment of the requirements for the degree of

MASTER OF SCIENCE

Major: Agricultural Meteorology

Program of Study Committee:
Raymond Arritt, Major Professor
Eugene Takle
Susanga Goggi
Petrutza Caragea

Iowa State University

Ames, Iowa

2007

TABLE OF CONTENTS

LIST OF FIGURES

CHAPTER 1. General Introduction

1.1 Overview

Genetically modified (GM) crops have been developed to improve crops in a variety of ways including resistance to pests and disease (James et al, 2003), increasing the quantity and quality of yields, and raising the tolerance levels of crops to stressful conditions such as drought or cold (Wang et al, 2003). While many of the effects of these GM crops are beneficial, there are also negative effects that have arisen since their creation. For example, the genetic purity of conventional crops is threatened by the possibility of cross-pollination from GM crops.

By predicting the movement and viability of pollen, we can begin to examine the risk of cross-pollination. Numerical simulation is a tool that can provide predictions of the dispersion of pollen from a source plot. We use the Lagrangian approach to modeling dispersion, which predicts the trajectories of individual pollen grains. Releasing a realistic number of pollen grains from a source field is nearly impossible due to computational limitations of the model, but by releasing a large enough number of particles in the model, we can obtain an accurate representation of pollen movement.

Maize (*Zea mays*) relies on the wind to carry pollen from its release point at the anther to a receptive silk. Since chances are small for any individual pollen grain to land on a receptive silk, reproduction in maize is dependent on releasing a large amount of pollen. Controlling and containing the pollination of maize can be extremely difficult due to the sheer number of pollen grains that are released, which is on the order of millions of grains per plant (Uribelarrea et al, 2002).

While our Lagrangian dispersion model (LDM) is able to predict the movement and viability of pollen, it is dependent on the accurate input of meteorological data. Predicting the movement of pollen requires modeling the three dimensional wind fields and the effects of turbulent eddies that dominate the daytime boundary layer while predicting viability requires modeling fields of atmospheric temperature and water vapor to determine the rate at which the viability of each pollen grain is lost. For these studies, we perform Large Eddy Simulation (LES) using the Advanced Regional Prediction System (ARPS).

The ARPS model was developed at the Center for Analysis and Prediction of Storms (CAPS) to

model and study a variety of weather processes on numerous scales (Xue et al 2000, 2001). ARPS has been used to study mesoscale or cloud-scale features, but has had little application in LES. Studies using ARPS as an LES model have used grid spacings from 2 m (Dupont, 2006) to 150 m (Chow et al, 2006). Although model results from these studies have exhibited turbulence statistics that are generally consistent with observations, some additional testing of ARPS to check that turbulent heat flux and development of the boundary layer are realistic should be performed to ensure accurate modeling of processes such as pollen dispersion that are generally confined to the boundary layer.

1.2 Lagrangian Modeling

Once environmental variables have been predicted, the output from ARPS is used by a Lagrangian Dispersion Model (LDM) to predict the dispersion and viability of maize pollen. The LDM is a stochastic model which makes use of Markovian processes.

The benefits of modeling the dispersion of particles in a Lagrangian rather than a Eulerian framework are in the treatment of dispersion. In a Eulerian model, the concentration of particles at any given point is treated as a scalar quantity that can be described by a conservation equation given by

$$\frac{\partial c}{\partial t} + u_i \frac{\partial}{\partial x_i} c = \frac{\partial}{\partial x_i}(\kappa \frac{\partial}{\partial x_i} c) \tag{1.1}$$

Wilson and Sawford (1985) point out that this equation requires the length scale of turbulence to be small compared to the length scale of particle dispersion. This assumption is violated for particles located near the source, as well as in regions with complex flow within a crop canopy (Wilson and Shaw, 1977). This is a drawback of using the Eulerian method to model pollen dispersion, considering that the majority of pollen is deposited within a few tens of meters from the source field (Emberlin et al, 1999, Hansen-Jesse and Obbrycki, 2000).

In Lagrangian models, the conceptual equation to find concentration is given as

$$c(x,t) = \int_{-\infty}^{t} \int_{V} P(x,t,x',t') S(x',t') dx' dt' \tag{1.2}$$

where V is the volume of the fluid being modeled, in this case the atmosphere, P(x,t,x',t') is the probability density for the position x at time t for particles released from x' at time t', and S(x',t') is the source strength (Tennekes and Lumley, 1972). This method has the advantage of modeling the concentration at any point exactly.

Rather than predict dispersion using a defined probability function, we release particles whose motions are simulated as Markov chains using a random flight model. Markov chains make implicit use of

the Langevin equation which describes the motion of a fluid particle that undergoes random accelerations (Legg and Raupach, 1982). Legg (1982) showed that this type of model could simulate the dispersion of particles from an elevated line source when compared to wind tunnel experiments. However, Wilson et al (1981) demonstrated that regions where there is a large variation in vertical velocity with height, such as a crop canopy, particles can experience an unrealistically large amount of downward motion and deposition.

The Langevin equation is given in Wilson and Sawford (1996) as

$$du = a(x, u, t)dt + b(x, u, t)d\epsilon \tag{1.3}$$

where a and b are the drift and diffusion terms, respectively, defined as

$$a = \frac{1}{T_L} = \frac{2\sigma_u^2}{C_0\epsilon} \tag{1.4}$$

$$b = (C_0\epsilon)^{1/2} \tag{1.5}$$

and $d\epsilon$ is a Gaussian white noise function with a mean of zero and variance equal to dt.

The Langevin equation has been shown in previous studies to provide realistic dispersion of particles (Sawford, 1998; Mito and Hanratty, 2002; Heppe, 1998). In addition, Heppe (1998) showed that the dispersion of fluid particles using the Langevin equation performed nearly as well as direct numerical simulation, which resolves all scales of turbulence down to the viscous scales, making it the most realistic simulation possible.

1.3 Thesis Organization

This thesis is divided into four chapters, with the third chapter being submitted for publication. The second chapter tests ARPS for use as a large-eddy simulation model. Although it has been written as a LES capable model, some additional testing is necessary to ensure its accuracy for LES. The treatment of turbulent heat flux in the atmosphere is diagnosed and checked for consistency with expected boundary layer behavior. The third chapter examines the problem of maize pollen dispersion and gives results from the ARPS/LDM model for the distribution and viability of pollen throughout the atmospheric boundary layer, as well as the concentration and viability of pollen upon deposition. General conclusions are given in the fourth chapter.

1.4 References

Chow, F. K., A. P. Weigel, R. L. Street, M. W. Rotach, and M. Xue, 2006: High-resolution large-eddy simulations of flow in a steep Alpine valley. Part I: Methodology, verification, and sensitivity studies. *J. Appl. Meteor.,* **45**, 63-86.

Dupont, S., V. d'Ornon, and Y. Brunet, 2006: Large-eddy simulation of forest edge flow with ARPS. *27th Conf. on Ag. For. Meteor.,* San Diego, CA, Amer. Meteor. Soc., CD-ROM, JP2.2.

Heppe, B. M. O., 1998: Generalized Langevin equation for relative turbulent dispersion. *J. Fluid Mech.* **357**, 167-198.

Hansen-Jesse, L. C., and J. J. Obrycki, 2000: Field deposition of Bt transgenic corn pollen: lethal effects on the monarch butterfly. *Oecologia,* **125**, 241-248.

James, D., A.-M. Schmidt, E. Wall, M. Green, and S. Masri, 2003: Reliable detection and identification of genetically modified maize, soybean, and canola by Multiplex PCR analysis. *J. Agric. Food Chem.,* **51**, 5829-5834.

Legg, B. J., 1983: Turbulent dispersion from an elevated line source: markov-chain simulations of concentration and flux profiles. *Quart. J. Roy. Meteorol. Soc.,* **109**, 645-660.

Legg, B. J., and M. R. Raupach, 1982: Markov-chain cimulation of particle dispersion in inhomogeneous flows: the mean drift velocity induced by a gradient in eulerian velocity variance. *Bound.-Layer Meteorol.,* **24**, 3-13.

Mito, Y., and T. J. Hanratty, 2002: Use of a modified Langevin equation to describe turbulent dispersion of fluid particles in a channel flow. *Flow Turbul. Combust.* **68**, 1-26.

Sawford, B. L., 1998: Reynolds number effects in Lagrangian stochastic models of turbulent dispersion. *Phys. Fluids* **3**, 1577-1586.

Tennekes, H., and J. L. Lumley, 1972: *A first course in turbulence.* MIT Press, Cambridge, MA.

Uribelarrea, M., J. Carcova, M. E. Otegui, and M. E. Westgate, 2002: Pollen production, pollination dynamics, and kernel set in maize. *Crop Sci.,* **42**, 1910-1918.

Wang, W., B. Vinocur, and A. Altman, 2003: Plant responses to drought, salinity and extreme temr-peratures: towards genetic engineering for stress tolerance. *Planta,* **218**, 1-14.

Wilson, J. D., and B. L. Sawford, 1996: Review of lagrangian stochastic models for trajectories in the turbulent atmosphere. *Bound.-Layer Meteorol.,* **78**, 191-210.

Wilson, J. D., G. W. Thurtell, and G. E. Kidd, 1981: Numerical simulation of particle trajectories in inhomogenous turbulence. *Bound.-Layer Meteorol.,* **21**, 423-441.

Wilson, N. R., and R. H. Shaw, 1977: A higher-order closure model for canopy flow. *J. Appl. Meteorol.,* **15**, 1198-1205.

CHAPTER 2. Vertical Profiles of Heat Flux

Abstract

The accuracy of Large Eddy Simulation (LES) depends on the ability to realistically model turbulent heat flux. Turbulent heat flux impacts the development of the atmospheric boundary layer by transferring heat throughout the layer and contributing to its growth. We test the Advanced Regional Prediction System (ARPS) for consistency with observed boundary layer development at three different vertical grid spacings to determine its suitability as a LES model. Vertical profiles of resolved and unresolved heat flux divergence are used to calculate the heating rate of the atmosphere and measures of boundary layer depth are compared to ensure accurate growth and development. Heating rate is modeled to remain constant through the boundary layer and decrease in magnitude over time, which is consistent with expected boundary layer behavior.

2.1 Introduction

The ability to accurately model turbulent fluxes within the atmosphere is necessary for an accurate representation of the atmospheric boundary layer. Since the characteristics of the boundary layer depend on the mixing of the atmosphere, accurately modeling the movement of momentum, heat and water vapor are vital components in Large Eddy Simulation (LES).

The development of the boundary layer dictates the depth of the atmosphere that is directly affected through surface heating and represents the region of the atmosphere where turbulence has a large impact on small-scale motions. On clear days, the surface is heated through solar radiation and then transfers some of that heat to the atmosphere. The boundary layer primarily acts to redistribute the heat through the lower atmosphere, generating a heat flux.

Variations in surface characteristics can have a profound impact on heat fluxes between the surface and the atmosphere and within the atmosphere itself (Segal and Arritt, 1992, Doran et al, 1995, Avissar and Liu, 1996). Accurate modeling of the surface and surface fluxes can directly impact predicted

atmospheric fluxes. Chow et al (2005) reported that modeled momentum fluxes in the atmosphere were reduced in their simulation as a result of underpredicted momentum flux at the surface.

Mason (1988) examined the effects of grid spacing and domain size on the fluxes of horizontal and vertical momentum using LES and reported that changes in either domain size or grid spacing had small effect on the results of the model. The one difference that was noted was coarser runs reported maxima and minima that were lower in magnitude, but he hypothesized that these changes were due to the coarseness of the model grid rather than error in the model.

The effects of varying the vertical grid spacing on heat flux profiles using LES will be studied. This will be accomplished by examining profiles of vertical heat flux divergence at various times during the afternoon as well as the overall development of the planetary boundary layer as determined from profiles of resolved heat flux. The next subsection will describe the LES model used. Subsection 3 will present results and discussion, and conclusions will be given in subsection 4.

2.2 Methods and Model

2.2.1 LES

LES was first used to model the atmospheric boundary layer in the early 1970s, when Deardorff (1972) simulated atmospheric turbulence for neutral and unstable boundary layers. Since that time, computing power has increased and we are now able to use LES with grid spacings of tens or hundreds of meters.

LES explicitly computes all scales of turbulence larger than a chosen filter function. The filter function usually resides somewhere within the inertial subrange, which separates the scales of generation and dissipation of turbulence kinetic energy. For scales smaller than the filter function, LES uses a parameterization to model the effects of turbulent eddies. As the model grid spacing decreases, more scales of turbulence are resolved in the model. (Zhou et al, 2001)

When choosing a grid spacing for the model, we must consider the feature we are trying to model. Bryan et al (2003) suggested that a grid spacing two orders of magnitude less than the feature being modeled may be necessary for an accurate representation. For this study, we examine turbulence in the boundary layer. The largest turbulent eddies will be of a size equal to the maximum boundary layer depth, which is on the order of 1000 m, suggesting that our grid spacing should be of order 10 m.

2.2.2 ARPS

LES is performed using the Advanced Regional Prediction System (ARPS) which is described in detail in Xue et al. (2000, 2001). ARPS is a three-dimensional compressible, non-hydrostatic model. Subgrid-scale turbulence is parameterized using a 1.5 order accurate closure following Moeng and Wyngaard (1989). Advection was modeled using a centered-in-space finite difference method that is 4th order in the horizontal directions and 2nd-order in the vertical direction.

For this study, the horizontal dimensions of the model domain are defined by a 64 x 64 grid with 100 m spacing between grid points. The vertical domain is five kilometers deep for each simulation. The vertical grid spacing varied between simulations, using spacings of 20m, 50m and 100m, which will be referred to as DZ20, DZ50 and DZ100, respectively. Five kilometers is likely larger than is necessary for this study since most pollen is confined to the lowest 1-2 kilometers, but was chosen to ensure that the top boundary condition of the model would not interfere with the development of the flux profiles in the mixed layer. Model results were given at minute intervals averaged hourly.

The surface was considered to be a homogeneous cultivated region with a roughness length of 0.1 m, leaf area index of 2.5 m^3/m^2 and a vegetative fraction of 70%. Although it has been reported that variations in surface features can affect heat fluxes, Hechtel et al (1990) determined that a homogeneous surface heat flux was able to model the convective boundary layer nearly as well as complex patterns of surface heat flux. It was hypothesized that this may result from being unable to resolve the lowest surface layer or complex terrain characteristics.

The model is initialized at 12 UTC using the 12 UTC sounding from Davenport, IA for August 9, 2003. Conditions on this day were clear with sufficient surface heating to produce modeled mixed layers on the order of a kilometer or higher. The model was run for a period of 12 hours to capture the creation and development of the boundary layer throughout the day.

In addition to turbulent heat flux, fluxes of momentum and moisture are important atmospheric processes in the boundary layer. Momentum flux transfers kinetic energy out of the atmosphere to the surface and is generally constant and small in magnitude through most of the boundary layer. A typical momentum flux profiles has a peak near the surface, where the wind speed is reduced to zero by friction, and near the top of the mixed layer, where the wind speed transitions to the mean wind speed of the free atmosphere. Moisture flux represents the movement of moisture into, out of, and through the atmosphere. The source of atmospheric moisture is at the Earth's surface from which water is evaporated or transpired to the atmosphere during the day. The amount of atmospheric moisture is generally constant through the boundary layer and decreases above it.

ARPS has been shown in previous studies to accurately model various turbulent statistics that are important in LES. Profiles of momentum flux and momentum flux divergence were produced in Mechem et al (2005) for storm scale motions. Weigel et al (2004) modeled the moisture flux divergence for an alpine valley and found that ARPS measurements were in good agreement with observations. It has been pointed out that fluxes near rigid lateral model boundaries (Chow et al 2005) and near the surface (Skyllingstad and Wyjesekera 2004) are generally underpredicted since turbulent eddies cannot be fully resolved in these regions.

2.2.3 Calculation of Heat Flux Divergence

The instantaneous vertical flux of potential temperature at a point, which we will refer to as heat flux, is defined as $w\Theta$, where w is the vertical velocity and Θ is potential temperature. Each variable can be separated into mean and turbulent parts as

$$w = \overline{w} + w' \tag{2.1}$$

$$\Theta = \overline{\Theta} + \Theta' \tag{2.2}$$

where w and Θ are the instantaneous values at each point, the overbar denotes the mean value at each height, and the prime denotes fluctuations from the mean. Substituting for $w\Theta$ gives

$$w\Theta = w\Theta + w'\overline{\Theta} + \overline{w}\Theta' + w'\Theta'. \tag{2.3}$$

The previous equation can be simplified using Reynolds Averaging to

$$\overline{w\Theta} = \overline{w}\overline{\Theta} + \overline{w'\Theta'} \tag{2.4}$$

The first term on the right hand side of Equation 2.4 defines the advective heat flux and the second term is the turbulent heat flux. For conditions with a flat, homogenous terrain, $\overline{w} \cong 0$ within the boundary layer. With this assumption, the term $\overline{w\Theta}$ can be neglected (Stull, 1988).

In LES, the w' and Θ' can be split into resolved and unresolved components as

$$w' = w'_r + w'' \tag{2.5}$$

$$\Theta' = \Theta'_r + \Theta'' \tag{2.6}$$

where the subscript r represents the resolved portion of each variable and the double prime represents the unresolved portion. Substituting Equations 2.5 and 2.6 into Equation 2.4 and using Reynolds Averaging, the turbulent heat flux at a point is found to be

$$\overline{w'\Theta'} = \overline{w'_r\Theta'}_r + \overline{w''\Theta''} \tag{2.7}$$

where $\overline{w'_r\Theta'}_r$ represents the resolved portion of the heat flux and $\overline{w''\Theta''}$ is the parameterized or unresolved heat flux. The unresolved heat flux is especially important near the surface where the size of turbulent eddies is small enough that they cannot be captured by the model (Moeng, 1984).

The horizontally averaged heating rate at a given height z, neglecting processes relating to radiation and latent heating, can be written as

$$\frac{\partial\overline{\Theta}}{\partial t} = -\frac{\partial\overline{w'\Theta'}}{\partial z} = -\frac{\partial\overline{w'_r\Theta'_r}}{\partial z} - \frac{\partial\overline{w''\Theta''}}{\partial z} \tag{2.8}$$

By rearranging Equation 2.8, we can solve for the unresolved heat flux divergence, given as $\partial\overline{w''\Theta''}/\partial z$, since the heating rate, $\partial\overline{\Theta}/\partial t$, and the resolved heat flux divergence, $\partial\overline{w'_r\Theta'_r}/\partial z$, can be solved using model output.

To calculate the resolved heat flux divergence at each model level and output time, we must obtain values for spatially averaged resolved heat flux using.

$$< \overline{w'_r\Theta'_r} >= \frac{\Sigma\overline{w'_r\Theta'_r}}{nx * ny} \tag{2.9}$$

where nx and ny are the number of grid points in each of the horizontal directions and $<>$ represents a spatial average. These spatial averages are then averaged in time as

$$[< \overline{w'_r\Theta'_r} >] = \frac{\Sigma < \overline{w'\Theta'}_r >}{n_t} \tag{2.10}$$

where n_t is the number of times being averaged and the [ ] denotes a time average. For this study, mean values of spatially averaged resolved heat flux were found as hourly averages, with $n_t = 60$. For example, the 17 UTC heat flux divergence profiles were calculated using the spatially averaged resolved heat flux at each level between 16:30 and 17:29 UTC. Values for $\partial\overline{\Theta}/\partial t$ are found by taking the difference between the value of $\overline{\Theta}$ at the beginning and end of each temporally averaged period.

Plots used in this analysis are scaled to boundary layer depth at each time. Boundary layer depth is defined as the height where the resolved heat flux becomes negative. Although this definition excludes the entrainment layer, the exact level where heat flux reached its minimum could not be established with certainty. Using the level where heat flux equals zero slightly underpredicts the boundary layer height but gives more detail about boundary layer growth.

2.3 Results and Discussion

For each simulation, resolved, unresolved, and total heat flux divergence is plotted at 17, 19, and 21 UTC in Figures 2.1-2.3. The importance of the unresolved portion of the heat flux divergence is

evident in the lowest few model levels where the values increase near the surface. These large unresolved heat fluxes act to balance the lack of resolved heat flux near the surface and maintain a constant rate of boundary layer heating near the surface. The unresolved portion of the heat flux becomes less important higher in the boundary layer as values fall quickly to below zero above the first few model levels, but still acts to maintain the constant heating rate through the boundary layer.

The total heat flux divergence remains constant through the boundary layer for each run and each time before decreasing above the boundary layer, consistent with observations that the daytime boundary layer heats up evenly over its depth on days with strong radiative input. The total heat flux divergence is also observed to decrease in each of the three simulations with time. Each of the simulations exhibits a heating rate of nearly $2 \cdot 10^{-3}$ K s^{-1}at 12:00, $1.25 \cdot 10^{-3}$ K s^{-1}at 2:00 and $0.75 \cdot 10^{-3}$ K s^{-1}at 4:00. This indicates that the boundary layer is developing at approximately the same rate in each of the simulations despite changes in the vertical grid spacing. The decrease in heating rate with time can be expected for two reasons: 1) as the boundary layer depth increases, the same amount of heat input must be distributed over the entire depth, slowing down the rate of heating, and 2) the amount of energy per unit area incident on the ground is defined by Lambert's Cosine Law as

$$E_{incident} = E_o cos\Psi \tag{2.11}$$

where E_o is the amount of energy incident from the sun when it is normal to the Earth's surface, $E_{incident}$ is the amount of energy actually incident on the surface, and Ψ is the solar zenith angle, which equals 0° at local noon and 90° at sunrise and sunset. As the afternoon passes, less solar energy will be heating the ground as the cosine of the sun's angle with the ground surface decreases.

While the magnitude of total heat flux divergence is nearly the same in each of the three simulations, the magnitudes of the resolved and unresolved flux divergences are noticeably different as grid spacing changes. The smaller grid spacings produce resolved flux divergences at 17:00 UTC that are substantially smaller near the surface. Resolved heat flux divergence varies between $-1.15 \cdot 10^{-3}$ K s^{-1}using DZ20 to near zero in DZ100. The increased resolved heat flux divergence near the surface in DZ100 is a result of increased averaging which occurs with larger vertical spacing. The opposite scenario is present for unresolved heat flux divergence where values are higher for smaller grid spacing to balance the resolved heat flux divergence.

DZ50 and DZ100 are characterized by smooth profiles throughout the boundary layer, which is due in part to the larger vertical grid spacing. On the other hand DZ20 exhibits a wavy profile which results from the increased resolution of turbulence. However, the general shape of the profile remains the same,

indicating the general treatment of turbulence remains the same.

Alternatively, the finer resolution runs may suffer from anisotropy since dx≫dz for finer vertical resolution. Our grid boxes in DZ20 are becoming very rectangular rather than square since our horizontal grid spacing is five times the vertical grid spacing. The vertical motions of turbulence are more resolved, causing turbulence to be advected realistically in the vertical, but slower in the horizontal. The differences in the horizontal and vertical motions cause eddies to become elongated in the vertical.

Figure 2.4 shows the change in boundary layer height over the course of the simulation. Lower resolution runs initialized the development of a mixed layer later than higher resolution runs. The delay in creating a mixed layer is due to an inability of coarse resolution to resolve the mixed layer until it has reached a sufficient height. DZ50 and DZ100 have large jumps early in the simulation. The boundary layer height at 9:00 LST in DZ50 is 136 m before jumping to 387 m an hour later while DZ100 increases from 64 m at 10:00 LST to 587 m at 11:00. Each of these jumps represents the boundary layer increasing to a point where turbulent eddies can be resolved by the model.

Comparisons of potential temperature profiles at 17:00 LST were made to compare the accuracy of the three simulations against the observed profile (Figure 2.5). At this time, all three simulations predict potential temperature to be constant through most of the boundary layer and then increasing above the boundary layer. In the lowest kilometer, the simulations predict the temperature within one Kelvin of the observed temperature.

2.4 Conclusions

The ARPS model was run to examine differences in the generation and evolution of heat flux profiles between 14 and 22 UTC. The vertical spacing in each run was varied, using values of 20, 50 and 100m and hourly averages of heat flux divergence were computed and plotted.

The general evolution of vertical heat flux divergence in the atmosphere was simulated in each of the runs. The vertical heat flux divergence was observed to remain consistent through the depth of the boundary layer, which indicates a constant heat rate through the layer which is in good agreement with boundary layer theory. Vertical heat flux divergence also decreased with time, which agrees with the concept that the rate at which the boundary layer is heated during the day decreases due to its increasing size and the decrease in energy being input to the surface to heat the layer as the afternoon progresses.

Results from all of the cases show expected patterns of PBL evolution. DZ50 seems to produce the best results since boundary layer growth for this case was more consistent and realistic than in DZ100,

but profiles of heat flux divergence were smoother than in case DZ20. This may be due to limiting the affects of anisotropy in the model which results when the horizontal and vertical grid spacings differ. Although the vertical spacing is half the horizontal spacing, horizontal advection is being treated with a 4th-order equation and vertical advection with a 2nd-order equation. Since use of a higher-order differencing equation used to simulate advection is as effective as reducing the grid spacing, running the model with a vertical spacing that is half the horizontal spacing limits anisotropy affects.

In the early hours of the run, the depth of the PBL as measured from the heat flux profiles grew rapidly before tailing off in the afternoon hours. Each of the model runs also captured the PBL height reaching a maximum around the same time, though at differing heights. Model runs using a coarse resolution tended to develop their mixed layers later. In DZ100, a noticeable mixed layer developed approximately a full hour later than other runs. This can likely be attributed in part to larger grid spacing using averages over larger areas.

Coarser runs also produced slightly larger heights for PBL top. The PBL varied 150 m between DZ100 and DZ20. Coarse runs also seem to produce the maximum boundary layer height slightly earlier in the simulation. The quickness with which the PBL develops may be in part a response for the coarser runs to compensate for the slow development of the mixed layer early in the run.

In conclusion, the ARPS model appears to be capable of reproducing realistic development of the boundary layer and the processes relating to the mixing of heat with the layer while performing LES at fine grid scales. There are variations in the results depending on the choice of vertical grid spacing, but these problems seem minimized when the effects of anisotropy can be limited by choosing grid spacing and advection options that treat turbulent motions equally in the horizontal and the vertical directions.

2.5 References

Avissar, R., and Y. Liu, 1996: Three-dimensional numerical study of shallow convective clouds and precipitation induced by land surface forcing. *J. Geophys. Res.,* **101**, 7499-7518.

Bryan, G. H., J. C. Wyngaard, and J. M. Fritsch, 2003: Resolution requirements for the simulation of deep moist convection. *Mon. Wea. Rev.,* **131**, 2394-2416.

Chow, F. K., A. P. Weigel, R. L. Street, M. W. Rotach, and M. Xue, 2006: High-resolution large-eddy simulations of flow in a steep Alpine valley. Part I: Methodology, verification, and sensitivity studies. *J. Appl. Meteor.,* **45**, 63-86.

Deardorff, J. W., 1972: Numerical investigation of a neutral and unstable planetary boundary layers. *J. Atmos. Sci.*, **29**, 91-115.

Doran, J. C., W. J. Shaw, and J. M. Hubbe, 1995: Boundary layer characteristics over areas of inhomogeneous surface fluxes. *J. Appl. Meteor.,* **34**, 559-571.

Dupont, S., V. d'Ornon, and Y. Brunet, 2006: Large-eddy simulation of forest edge flow with ARPS. *27th Conf. on Ag. For. Meteor.,* San Diego, CA, Amer. Meteor. Soc., CD-ROM, JP2.2.

Hechtel, L. M., C. H. Moeng, and R. B. Stull, 1990: The effects of nonhomogeneous surface fluxes on the convective boundary layer: A case study using large-eddy simulation. *J. Atmos. Sci.*, **47**, 1721-1741.

Mason, P. J., 1989: Large-eddy simulation of the convective atmospheric boundary layer. *J. Atmos. Sci.*, **46**, 1492-1516.

Moeng, C. H., 1984: Statistics of conservative scalars in the convective boundary layer. *J. Atmos. Sci.*, **41**, 3161-3169.

Moeng, C. H., and J. C. Wyngaard, 1989: Evaluation of turbulent transport and dissipation closures in second-order modeling. *J. Atmos. Sci.*, **46**, 2311-2330.

Segal, M., and R. W. Arritt, 1992: Non-classical mesoscale circulations caused by surface sensible heat flux gradients. *B. Am. Meteorol. Soc.,* **73,**, 1593-1603.

Stull, R. B., 1989: *An Introduction to Boundary Layer Meteorology.* Kluwer Academic Publications, 666 pp.

Xue, M., K. K. Droegemeier, and V. Wong, 2000: The Advanced Regional Prediction System (ARPS) - A multiscale nonhydrostatic atmospheric simulation and reiction tool. Part I: Model dynamics and verification. *Meteor. Atmos. Phys.,* **75**, 161-193.

Xue, M., K. K. Droegemeier, V. Wong, A. Shapiro, K. Brewster, F. Carr, D. Weber, Y. Liu, and D.-H. Wang,2001: The Advanced Regional Prediction System (ARPS) - A multiscale nonhydrostatic atmospheric simulation and prediction tool. Part II: Model physics and applications. *Meteor. Atmos. Phys.,* **76**, 134-165.

Zhou, Y., J. G. Brasseur, and A. Juneja, 2001: A resolvable subfilter-scale model specific to large-eddy siulation of under-resolved turbulence. *Phys. Fluids,* **13**, 2602-2610.

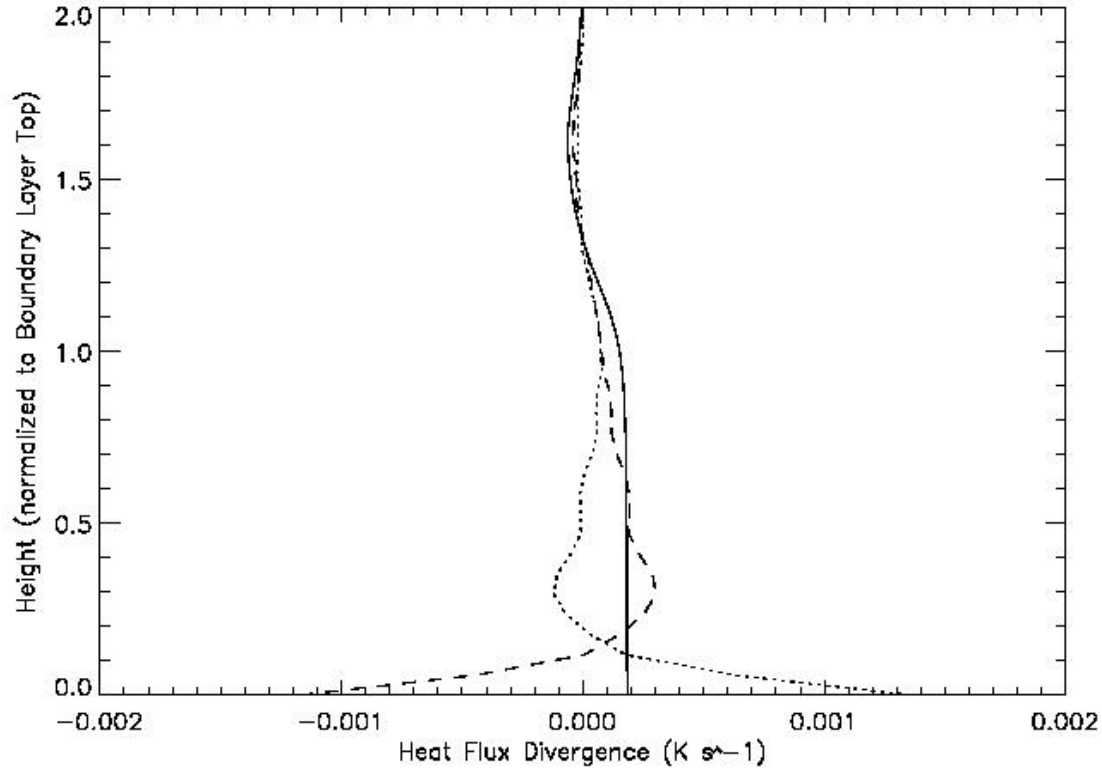
2.0
1.5
1.0
0.5
0.0
Height (normalized to Boundary Layer Top)
−0.002
−0.001
0.000
0.001
0.002
Heat Flux Divergence (K s^−1)

(a)

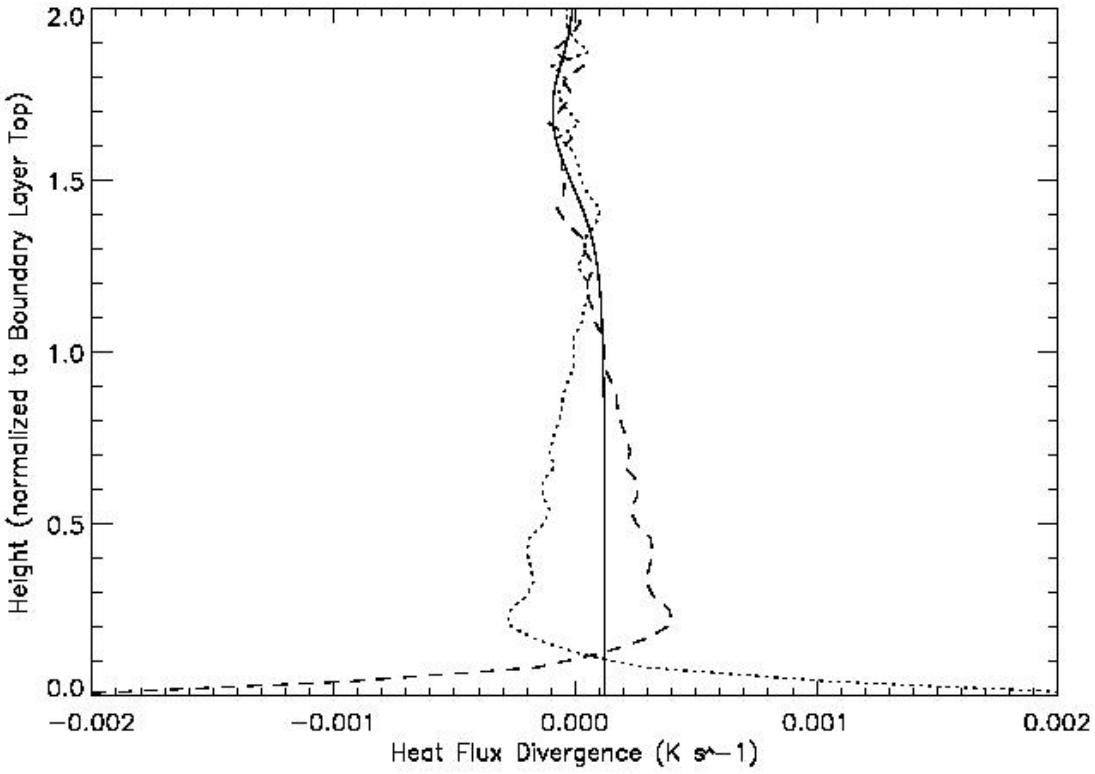
2.0
1.5
1.0
0.5
0.0
Height (normalized to Boundary Layer Top)
−0.002
−0.001
0.000
0.001
0.002
Heat Flux Divergence (K s^−1)

(b)

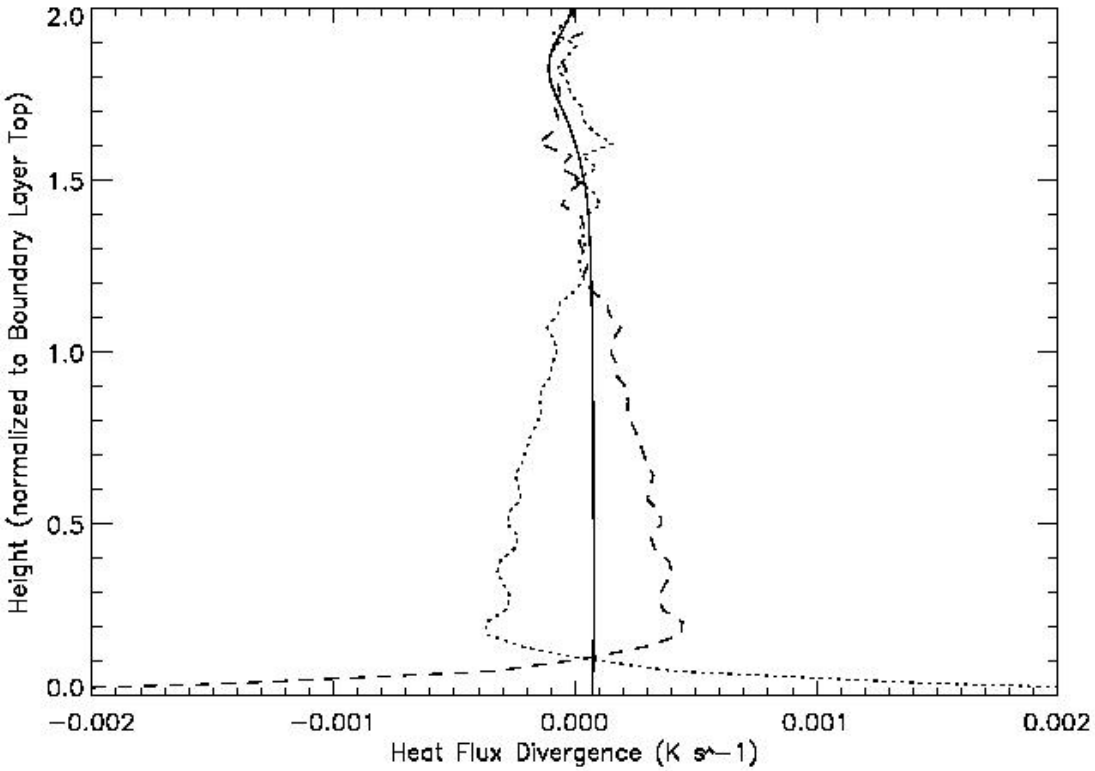

(c)

Figure 2.1 Profiles of vertical heat flux divergence for 11:00 (a), 13:00 (b) and 15:00 LST (c) for DZ20

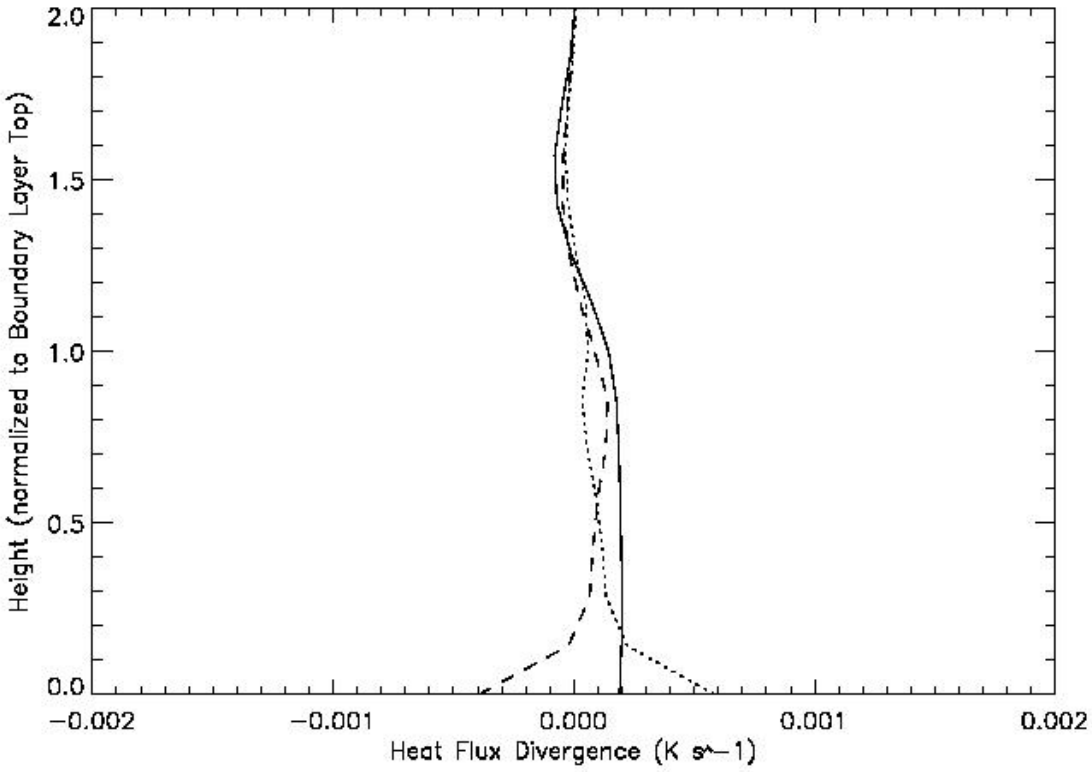
2.0
1.5
1.0
0.5
0.0
Height (normalized to Boundary Layer Top)
−0.002
−0.001
0.000
0.001
0.002
Heat Flux Divergence (K s^−1)

(a)

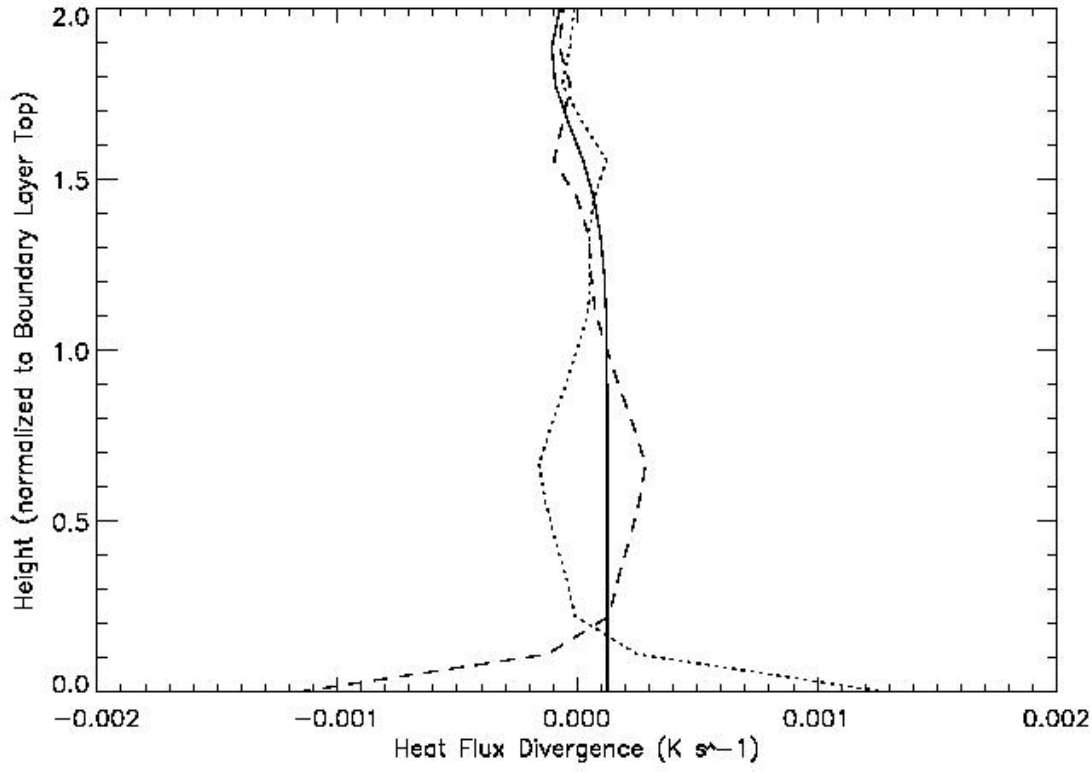
2.0
1.5
1.0
0.5
0.0
Height (normalized to Boundary Layer Top)
−0.002
−0.001
0.000
0.001
0.002
Heat Flux Divergence (K s^−1)

(b)

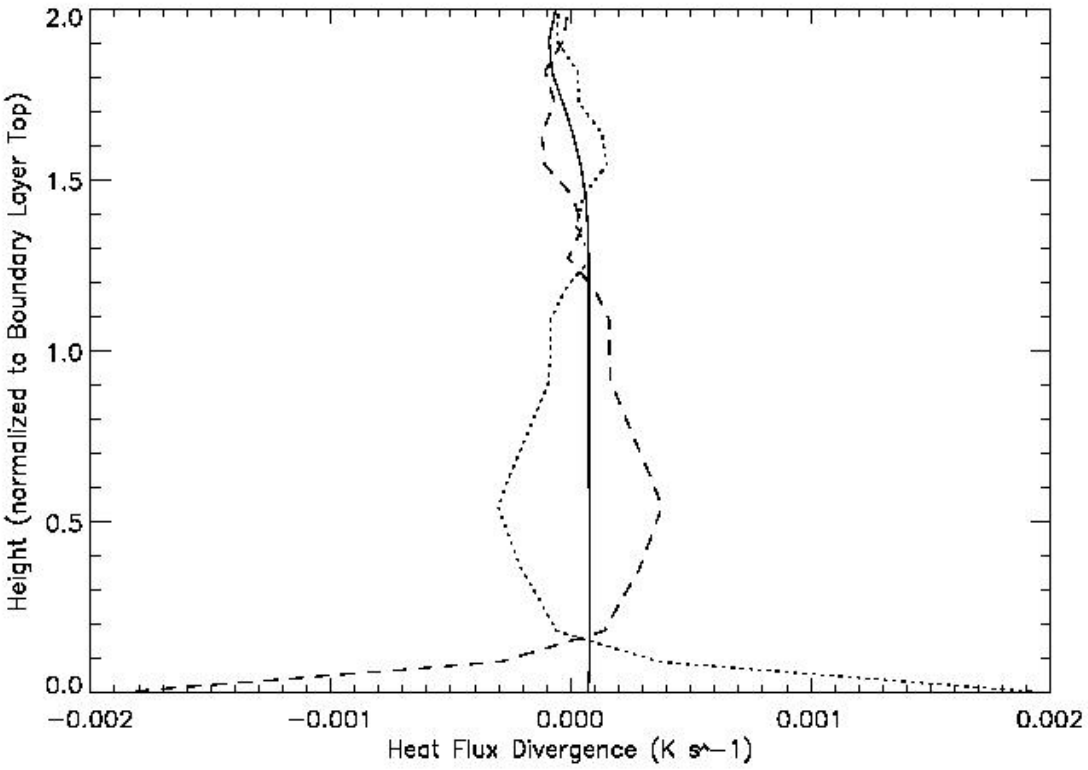

(c)

Figure 2.2 Profiles of vertical heat flux divergence for 11:00 (a), 13:00 (b) and 15:00 LST (c) for DZ50

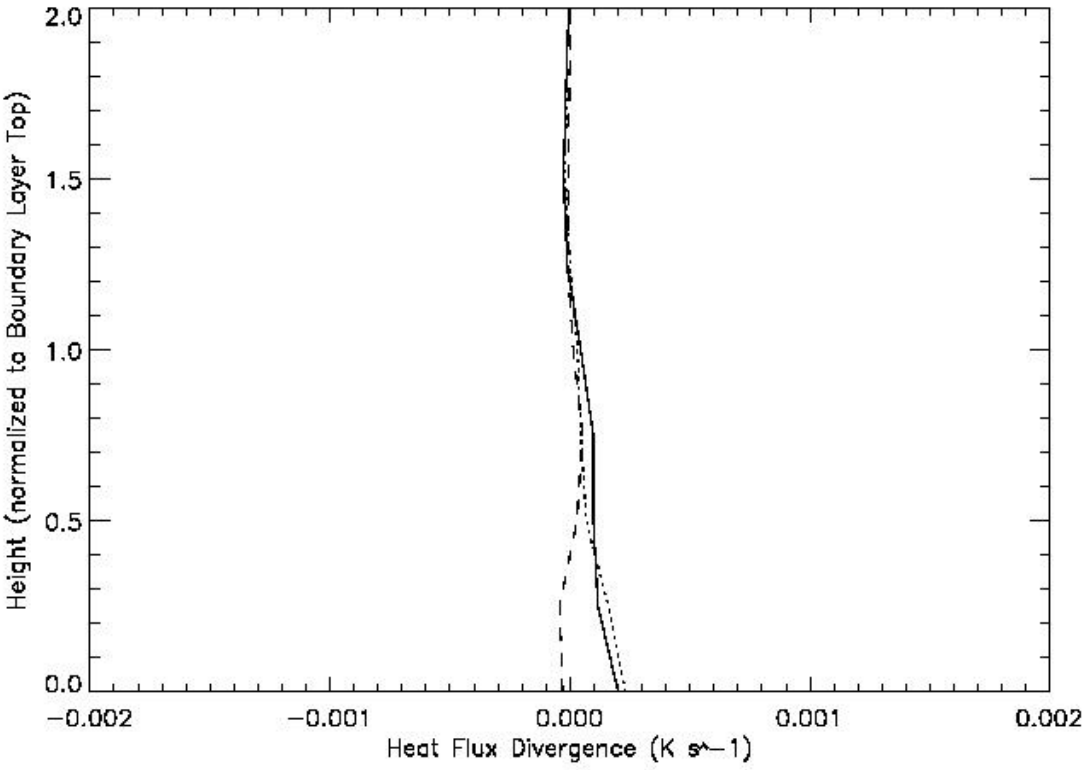
Height (normalized to Boundary Layer Top)
2.0
1.5
1.0
0.5
0.0
−0.002
−0.001
0.000
0.001
0.002
Heat Flux Divergence (K s^−1)

(a)

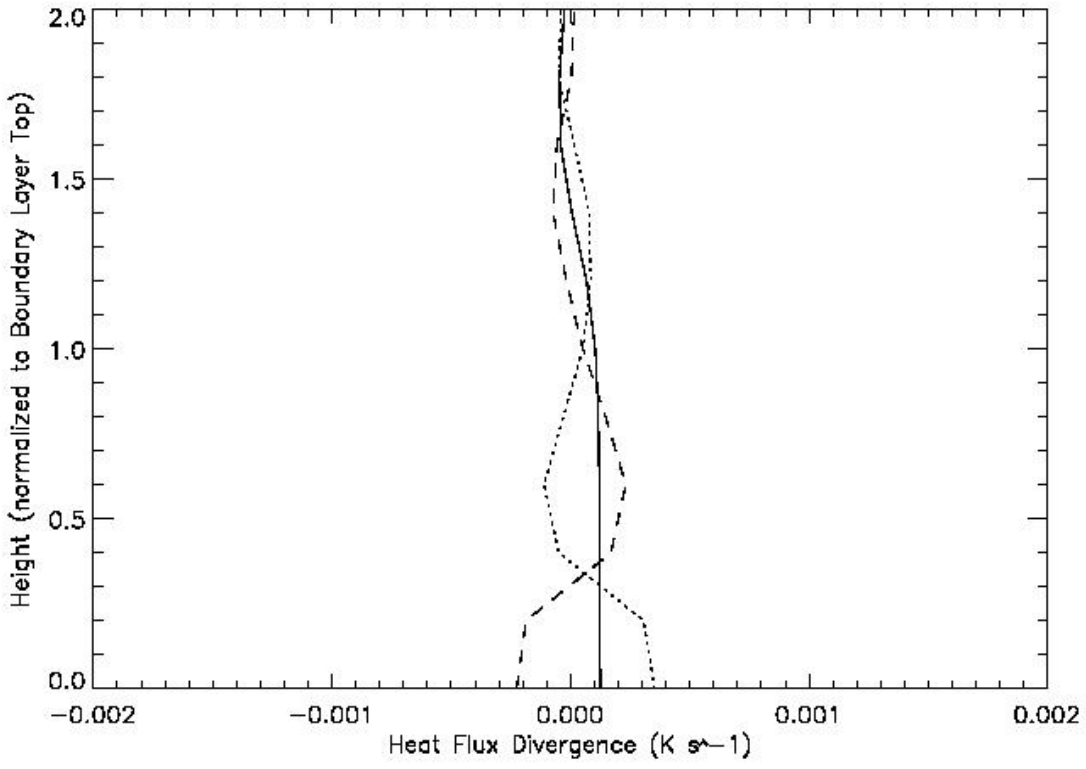
Height (normalized to Boundary Layer Top)
2.0
1.5
1.0
0.5
0.0
−0.002
−0.001
0.000
0.001
0.002
Heat Flux Divergence (K s^−1)

(b)

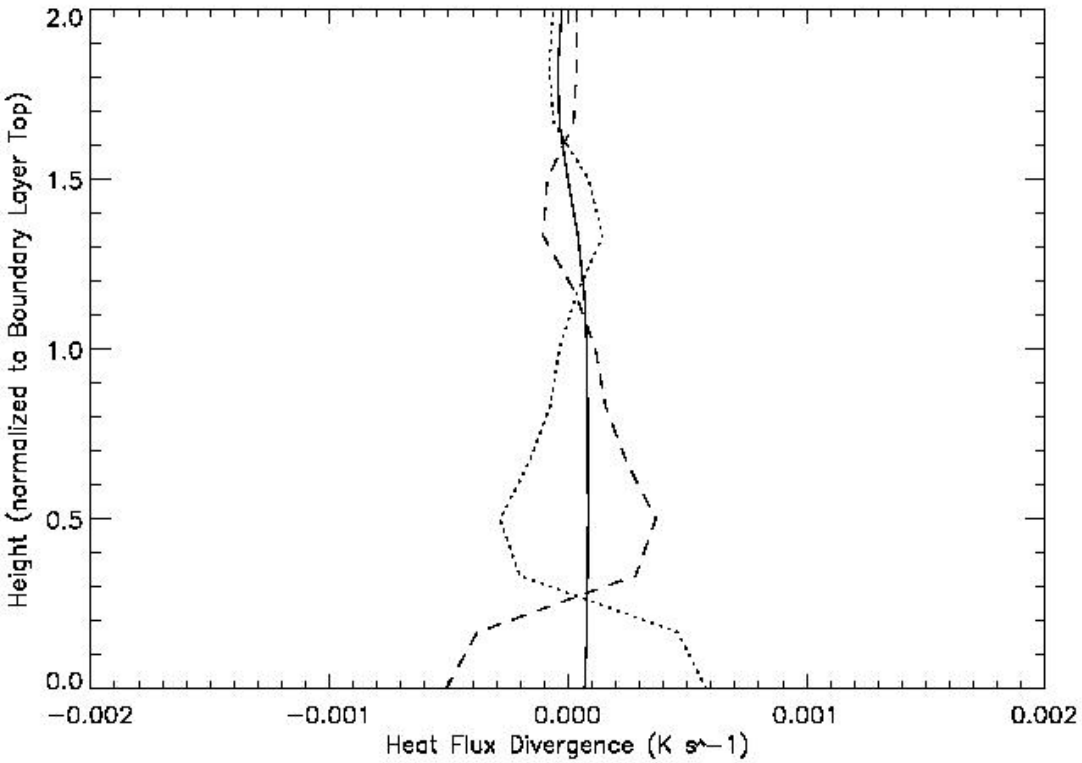

(c)

Figure 2.3 Profiles of vertical heat flux divergence for 11:00 (a), 13:00 (b) and 15:00 LST (c) for DZ100

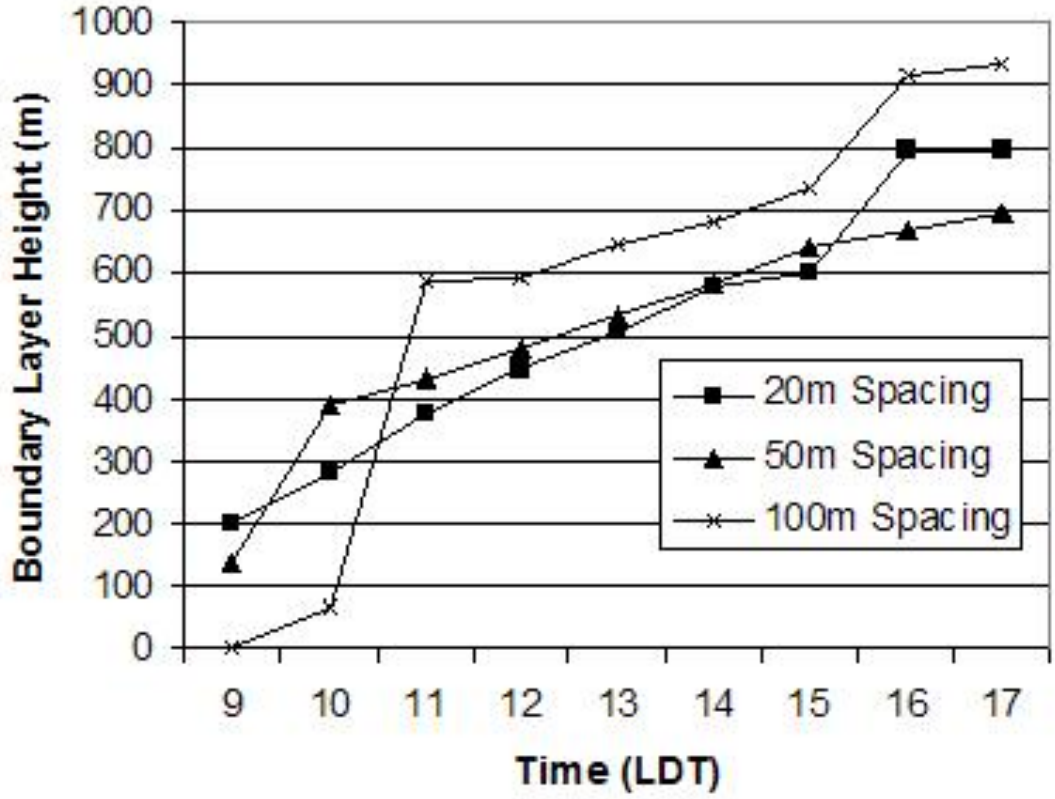

Figure 2.4 Change in boundary layer height over the course of the simulations

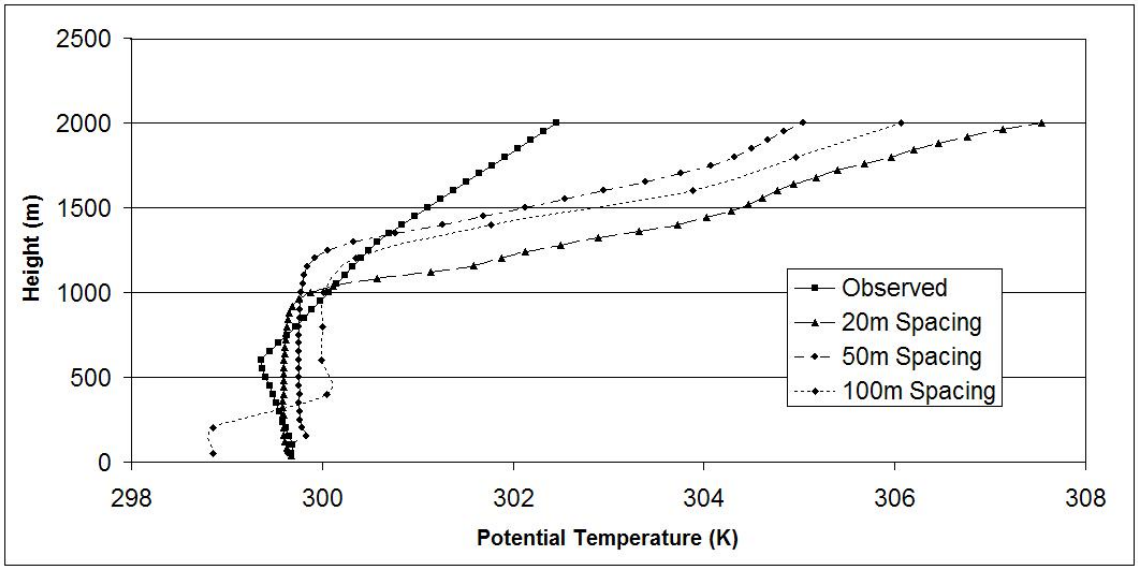

Figure 2.5 Profiles of Potential Temperature at 17:00 LST

CHAPTER 3. The dispersion and viability of maize pollen

Abstract

The creation of genetically modified (GM) crops has raised concerns regarding the transfer of genes from GM crops to wild relatives. To assess the risk of outcross, the development of numerical models that can accurately predict the movement depositional viability of pollen is needed. In maize, the primary mode of pollination is the transport of pollen by wind. Large Eddy Simulation (LES) is a tool to model turbulent motions that have the potential to lift pollen high into the atmospheric boundary layer and transport it over distances of at least five kilometers.

A LES model has been combined with a Lagrangian Dispersion Model to predict the transport and viability of pollen in the atmosphere. Predictions have been made for the deposition of maize pollen and of pollen viability upon deposition, as well as for vertical profiles of concentration and viability through the boundary layer. Viable pollen is modeled to be distributed throughout the boundary layer and transported over five kilometers before reaching the ground.

3.1 Introduction

With the development of genetically modified (GM) crops, concerns have been raised regarding the potential for cross-pollination between GM crops and their wild relatives. The rapid increase in the amount of GM crops worldwide has prompted regulations to be enacted in a number of countries (Nap et al 2003). To better create policy, a thorough examination of the problem is necessary, which will require numerous field studies and numerical simulations.

In maize (*Zea mays*), pollination requires that viable pollen released from the anther land on a receptive silk. Timing is critical for successful pollination to occur (Ma et al 2004). Previous studies as early as Peterson (1942) and Lohnquist and Jugenheimer (1943) have shown that maize pollen must land on a silk while it is receptive to produce a kernel. More recently, Basetti and Westgate (1993a, 1993b) determined the length of time that silks would be optimal for receiving pollen was seven days and may be less under adverse conditions.

Maize produces a characteristically large pollen grain with a diameter of approximately 90 microns and terminal fall speed ranging from approximately 20 cm s^{-1}(Raynor et al 1972) to 32 cm s^{-1}(Aylor 2002) depending on the mass of the pollen grain. Due to its high terminal velocity, most maize pollen settles within a few meters from its release point. This pattern has been observed in observational studies by Aylor (2003) and Bullock and Clarke (2000). Raynor et al (1972) observed that the majority of pollen was deposited within its source field and that deposition 60 m away from the source field was less than 1% of the value observed at a distance of 1m.

In order to cross-pollinate, pollen must be transported from its source field to another field. While there is evidence that some portion of pollen transport in maize is caused by insects, the primary mode of transportation is by wind (Emberlin 1999, Klein et al 2003). In order for pollen to travel far enough from the source field to pose a threat for cross-pollination, there must be a process taking place that can produce sufficiently large vertical velocities to counteract the large settling speed of pollen (Brunet et al 2001, Wilson et al 2004). This is supported by observations of pollen throughout the atmospheric boundary layer. Brunet et al (2001), herein referred to as B01, observed viable pollen present throughout the boundary layer at various times during the day, which may allow pollen to travel tens of kilometers.

Viability is generally defined as having the capacity to live, grow, germinate or develop (Lincoln et al. 1982). The viability of maize pollen has been found to be directly linked to the water content of the pollen grain (Aylor 2003, Fonseca and Westgate 2005). Barnabus (1985) found that maize pollen began to lose its ability to pollinate another plant once it lost over 50% of its initial moisture, and the physiology of the pollen was affected once it lost 80% of its original water content. Kerhoas et al (1987) also reported a significant loss of viability once half of the initial pollen moisture content was lost.

Viability is influenced by a number of outside factors, specifically the temperature and water potentials of the plant as well as the atmosphere (Schoper et al 1987). Higher atmospheric temperature and lower atmospheric water potential both tend to produce pollen with reduced viability (Luna et al, 2001, Schoper et al 1987). Fonseca and Westgate (2005) observed that pollen tended to lose half of its moisture content after one hour when exposed to warm, dry conditions, but only lost one quarter of its moisture content under cool, moist conditions in that time. Aylor et al (2004) observed pollen to remain viable for over three hours using in vitro methods of germination, and argued that pollen viability may not be a limitation to outcross.

Most measures of pollen lifetime have been taken at surface conditions of temperature and atmospheric water content. Atmospheric conditions can vary through the boundary layer, and this may have an impact on the longevity of pollen. Given a typical sounding for summer in the Midwest, the vapor

pressure deficit and resulting lifetime of pollen can be estimated (Figure 3.1). Within the boundary layer, temperature is observed to decrease with height, while moisture content remains constant. This causes the vapor pressure deficit to decreases with height, slowing the rate of water loss from pollen grains higher in the boundary layer. These estimates indicate that, in theory, pollen that is lifted through the boundary layer should be able to remain viable much longer than pollen that is confined near the surface.

Should a pollen particle survive to be deposited in a neighboring field, it must then compete with the pollen released from that field to pollinate a plant. Some varieties of maize can produce upwards of $3{\cdot}10^6$ pollen grains per plant during periods of peak pollen shed (Uribelarrea et al, 2002). Uribelarrea et al (2002) observed that the amount of pollen released per plant decreased as plant density increased, but that the total pollen released per square meter remained similar. The density of pollen around a field makes it difficult for pollen from a separate source field to pollinate plants in that field. The likelihood that GM pollen will manage to pollinate a wild relative should decrease with distance from the GM field, since pollen deposition decreases rapidly away from the source field.

Quantifying the maximum distance with risk of cross-pollination from a given source field has been the subject of a number of field studies. Luna et al (2001) observed that no outcrossing took place in any fields farther than 300 m from their source field, but hypothesized that pollen could potentially travel much farther. Ma et al (2004) observed that less than 1% of genetically modified maize successfully pollinated another plant beyond 30 m, and concluded that an isolation distance of 200 m around fields of GM maize should be sufficient to prevent outcross.

To determine effective isolation distances for GM crops, accurate models are needed to predict the dispersion, deposition and risk of outcross. Such a model would need to predict the turbulent wind fields throughout the boundary layer, as well as the temperature and water vapor profiles in the atmosphere. To do this, we employ the use of Large Eddy Simulation (LES), using the Advanced Regional Prediction System (ARPS), combined with a Lagrangian Dispersion Model (LDM).

The next section discusses the models and equations used in this study. The third section will present results from two field studies and the corresponding model simulations. The fourth section will provide a discussion of the results, and the final section will provide conclusions from this work.

3.2 Methods and Models

3.2.1 Large Eddy Simulation

To obtain accurate predictions of pollen flow, we would need to perform Direct Numerical Simulations, which explicitly resolve all scales of turbulence. However, Direct Numerical Simulation is extremely complex and time consuming, making it an unattractive choice. A widely accepted compromise is LES, which was first used to model the atmospheric boundary layer when Deardorff (1972) simulated atmospheric turbulence for neutral and unstable boundary layers. Since that time, computing power has increased significantly, and we are now able to use LES at grid scales on the order of hundreds or even tens of meters.

LES functions by explicitly computing all scales of turbulence in the atmosphere larger than a chosen filter function, which is dependent on the scale of the model grid. The scale of the filter function is usually found within the inertial subrange, which separates the scales of generation and dissipation of turbulence kinetic energy. For turbulent scales smaller than the filter, LES uses a parameterization to model the effect of turbulent eddies on the atmosphere.

3.2.2 LDM

The LDM predicts movement of pollen or other particles in the atmosphere given input fields of u, v, and w, which represent wind in the x, y and z directions, and values for turbulence kinetic energy. The source field is characterized as a square, approximately 75m on a side. The timestep of the model was 0.5 s, with pollen being released each timestep from approximately 650 source points within the field spaced throughout the field. The total amount of pollen that was released over the course of the simulation exceeded $3.26 \cdot 10^7$ grains.

The transport of pollen is treated as a Markov Chain, and is given by

$$x_{ik}(t + \delta t) = x_{ik}(t) + \delta t[u_{ik}(t) + u'_{ik}(t)], k = 1, 2, 3 \tag{3.1}$$

δ t is the timestep, u_{ik} represents the mean wind speed in the k direction on the ith particle as input to the model, and u'_{ik} is the simulated random component of the wind which accounts for subgrid turbulence. These turbulent motions are calculated as

$$u'_{ik}(t + \delta t) = u'_{ik}(t)R_{ik}(\delta t) + [1 - R_{ik}(\delta t)^2]^{1/2} q\sigma_{ik}, k = 1, 2, 3 \tag{3.2}$$

where R represents an autocorrelation value, q represents a normally distributed random number between zero and one, and sigma represents the standard deviation of the wind speed in the k direction. R acts

as a memory term of turbulence at the previous timestep.

In previous applications (Arritt et al, 2007), the LDM received input from a meteorological preprocessing program which used a single observation of wind speed combined with a measure of the surface roughness length to produce a logarithmic wind profile which was calculated as

$$u(z) = \frac{u_*}{k} ln \frac{z-d}{z_m} \tag{3.3}$$

Canopy effects on the wind field were included by modifying the wind field at levels within and above the canopy using

$$u(z) = u(h) * exp(a(\frac{z}{h} - 1)) \tag{3.4}$$

In the previous equations, u(z) is the wind speed at height z, u_* is the friction velocity, k is the van Karman's constant set to 0.4, d is the displacement height, or the height at which the wind speeds reaches zero, z_m is the roughness length of the surface, and h is the height of the crop canopy. The parameter a is an attenuation coefficient which is dependent on vegetation density. For the LDM, $a = 4$.

To simulate pollen dispersion over the course of a day, the LDM was run for one hour periods, using an hourly averaged wind speed to produce the wind profile. Results from each hour were combined to produce a prediction for the day. A drawback of using this method is that the mean wind for each hour long period is in one direction. Any vertical motions and deviations from the mean horizontal wind are produced from Equation 3.4.

A new method of giving input to the LDM is to perform LES using the ARPS model. Output from the ARPS model is produced each minute to provide an almost continuous stream of data to the LDM. The benefits that ARPS provides over the meteorological preprocessor is that more complex wind fields can be consistently input to the LDM and it does not require constant atmospheric measurements. The lack of measurements are also a drawback of ARPS since it has no other way of knowing the actual conditions as the day progresses. The prediction of pollen dispersion using ARPS is dependent on the accurate simulation of the daytime boundary layer.

One of the goals of this study is to compare the deposition results from simulations receiving input from the meteorological preprocessing program to runs that use ARPS output. In this report, the LDM coupled with the meteorological preprocessor will be abbreviated as Pre/LDM, and when coupled with ARPS will be abbreviated ARPS/LDM.

3.2.3 ARPS

ARPS is used to model the atmospheric variables necessary to predict pollen dispersion and viability: winds in three directions, turbulence kinetic energy, potential temperature and specific humidity. The ARPS model is a three-dimensional, compressible and non-hydrostatic model which is described in detail in Xue et al. (2000, 2001). Subgrid-scale turbulence is parameterized using K-theory and a 1.5 order closure following Moeng and Wyngaard (1989). Although designed for use as a mesoscale model, ARPS has been used in recent studies as an LES model with horizontal grid resolutions ranging from 2 m (Dupont, 2006) to 150 m (Chow et al, 2006).

For this study, the horizontal dimensions of the model are defined by a 103 x 103 point domain with 100 m spacing between grid points. The vertical domain was chosen to consist of 153 grid points spaced 50 m apart based on model results presented in Chapter Two. Model results were output at one minute intervals which are used as input for the LDM. The ground surface was considered to be a homogeneous cultivated region which is representative of the region where the field study was performed. The atmosphere in ARPS was initialized at 12 UTC using a single sounding and assuming that the atmosphere was horizontally homogenous. Since the field study was not performed near a sounding site, initialization for the model was created by averaging the 12 UTC soundings from Omaha, NE and Davenport, IA.

3.2.4 Pollen Viability

A number of equations have been used to determine how quickly maize pollen loses water content and viability. Aylor (2003) suggests a flux equation to describe the rate of water mass lost to the pollen based on the magnitude of the gradient of water vapor between the pollen grain and the atmosphere. For this study we use an empirical relationship that was developed by Fonseca and Westgate (2005). They proposed that the amount of water remaining in a pollen grain could be modeled as a function of the water vapor pressure deficit of the atmosphere. Vapor Pressure Deficit is calculated as a function of temperature and vapor pressure, given by

$$e_{sat,i} = 6.112 * exp(\frac{17.67 * (T_i - 273.15)}{(T_i - 273.15) + 243.5}) \tag{3.5}$$

$$e_i = (\frac{0.622}{q_{v,i} * \frac{p_i}{100}} + \frac{37.8}{p_i})^{-1} \tag{3.6}$$

$$VPD_i = (e_{sat,i} - e_i) * 0.01252 \frac{mb \cdot s}{mmhg \cdot min} \tag{3.7}$$

where T_i, p_i, q_i, $e_{sat,i}$ and E_i in Equations 3.5 and 3.6 are the temperature, pressure, atmospheric specific humidity, saturation vapor pressure and vapor pressure of the air surrounding the ith pollen grain. VPD_i is the vapor pressure deficit experienced by ith particle at any time step and the final term in Eq. 3.7 is a conversion from mb· s to mmHG· min. The accumulated vapor pressure deficit over time experienced by the airborne particle is calculated by:

$$VPDT_{t+1,i} = VPDT_{t,i} + VPD_i * \Delta t \tag{3.8}$$

Viability of the pollen grain is calculated as a function of the PMC as

$$PMC = 63.2 * exp(-b * VPDT_{t,i}) \tag{3.9}$$

In Equation 3.9, PMC is the pollen moisture content for the ith particle, b is an empirically derived constant of $1.2 * 10^{-3}$. The value of 63.2 in Equation 3.9 is assumed to be the percentage value of PMC that pollen has when it is initially released, which is in close agreement with studies done by Kerhoas et al (1987) and Rockel-Drevet and Digonner (1995).

The percent viability of pollen is given as

$$Viab = \frac{PMC - 28.8}{63.2 - 28.8} \tag{3.10}$$

Pollen is assumed to lose all viability when its PMC approaches the lower limit of 28.8, which corresponds to approximately 55% of its original water content.

3.3 Results and Discussion

3.3.1 Pollen Deposition

To gather observations and data of pollen dispersion, a field project was conducted near Ankeny, IA. Pollen was collected on pollen traps which were placed around the field at distances of 1, 10, 35,100, 150, 200, and 250 m from the field, shown in Figure 3.2. The smaller spacing of pollen traps near the source field is intended to capture the large gradient in deposition that has been observed in previous studies (e.g. Hansen-Jesse and Obrycki 2000).

Data from the pollen traps were collected for six days between 6-12 August 2003, and results are examined from Aug 8-11. Surface winds for each day are shown in Figure 3.3. Winds were between 1-3 m $s^{-1}$and were directed from the northeast on August 8 and from the east on August 9. August 10 exhibited lighter and more variable winds while August 11 returned to northeast winds ranging from 1-3 m s^{-1}.

Interpolated deposition from the pollen traps is shown in Figure 3.4. Interpolation was performed using a weighted distance function to estimate deposition at locations where no pollen traps were present.

Plots of the concentration of pollen deposition are shown in Figure 3.5 for August 8-11 using the Pre/LDM. The four modeled days are in good general agreement with the observations. On each day, the majority of pollen was deposited over the source field, with tails of pollen being deposited in the directions of the prevailing winds for each day. Despite changes in the wind speeds during successive days, the magnitude of pollen deposited in the region of the source field remained much the same over the four days. Deposition over the source field was slightly higher on August 10 and 11. On August 10, lower horizontal wind speeds are likely accountable for the higher source field deposition. August 11 experienced wind speeds that were at least as strong as the other days, but with less directional variation than other days.

Pollen was dispersed in three main plumes south and southwest of the source plot on August 8. August 9 had one main plume of pollen to the west of the source field, and three smaller plumes northwest and southwest of the field. On August 10 pollen was transported generally northeast with a some deposition north and east of the field. Winds returned out of the northeast on August 11, and pollen was moved in a large plume south and southwest.

Wind fields produced from the ARPS model are shown in Figure 3.6. With the exception of August 10, the modeled wind fields generally display less variation and slightly higher wind speeds than the observed winds, but do capture the general wind direction. The modeled wind field for August 10 shows very light winds predominately out of the northeast. Modeled winds with appreciable speed on August 10 are still out of the south or southwest.

Deposition predictions from the ARPS/LDM are shown for the near-field in Figure 3.7 and the far-field in Figure 3.8. The first two days of the study show very similar patterns to the observations and the results from the Pre/LDM, but only one main plume can be identified on each day. This results from increased variability of winds from the ARPS model compared with the meteorological preprocessor. Deposition on August 8 was primarily west and southwest of the source field. No pollen was deposited southeast of the field as was seen in the previous model combination. On August 9 and August 11 pollen was transported west and southwest, respectively, which is in good agreement with the observations. On August 10, the ARPS/LDM predicted a northward movement of pollen, which disagrees with both the Pre/LDM and the observations.

Plots of the far-field deposition indicate that an appreciable amount of pollen was transported at least five kilometers on most days. This is much farther than any field tests have been able to measure,

but has been hypothesized to be possible (Luna et al, 2001). Concentrations of pollen at this distance are low, which makes it difficult for pollen traveling this far to out-compete local pollen for silks.

Plots comparing the concentrations of pollen with distance from the field edge are given in Figure 3.9 for the primary direction of pollen transport for each day. Since the number of simulated particles is much smaller than the number of particles released from the field, the observations and model results were scaled to a maximum of 100 along the transect. While the observations from the pollen traps show a decrease in deposited pollen away from the source field, both models actually show a slight increase in deposition between 1 m and 10 m before decreasing. The only exception is August 10 when wind speeds were lowest. The increased deposition at 10 m in the models may be due to the increased release height of pollen in the model compared to the field study.

In addition to overpredicting the deposition next to the field, both models also tend to overpredict deposition at distances of a few hundred meters. The ARPS/LDM model has the higher prediction between the two models, which may be attributed to the additional vertical velocity input to the LDM model from ARPS. When combined with the treatment of random velocity components in the LDM, this can produce larger values for vertical wind speed to lift pollen into the atmosphere than would be possible using the preprocessor program.

3.3.2 Pollen Viability upon Deposition

The average viability of deposited pollen at each point in the model is shown in Figure 3.10. Viability decreases as pollen is deposited farther away from the source field. A large number of pollen grains retain their viability even after traveling over five kilometers from the source field. This would tend to agree with the assessment given by Aylor et al (2003) that pollen viability may not be a limiting factor to outcross potential.

Transects of pollen viability along the main axis of dispersion are given in Figure 3.11. Pollen viability drops off nearly linearly with distance despite the use of an exponential equation to describe the rate of viability loss. The cause of this contradiction is that the values between the maximum and minimum values of PMC (63.2 and 28.2, respectively) on the exponential curve can be reasonably approximated as linear (Figure 3.12). Using the assumption that viability drops off linearly with time, the transects of modeled pollen viability are reasonable; higher wind speeds will transport pollen farther in the same time, while viability falls off at the same rate. This is evident in the model predictions where the rate of viability decrease with distance is much lower on days with higher wind speeds (Aug. 11), and greater on days with lower winds (Aug. 10).

The maximum distance traveled by pollen still retaining at least half of its viability was approximately five kilometers on days with maximum wind speeds of 3-4 m s^{-1}. Assuming pollen traveled at a constant rate away from the field, it would take pollen traveling 3 m s^{-1}approximately 1700s to travel the distance of five kilometers. Assuming that pollen continues to lose its viability at an approximately linear rate, it can be expected to completely lose its viability approximately an hour after being released. This prediction matches results from Luna et al (2001) who observed pollen to lose all viability within 1-2 hours. It also means the additional lifespan of pollen lifted into the boundary layer may not be as significant as originally thought. It can also be concluded that, under moderately windy conditions of 3-4 m s^{-1}, the maximum range of viable pollen is approximately 10-15 kilometers.

3.3.3 Vertical Profiles

A separate field study was conducted by B01 by flying over a large area of maize fields. Ten flights were made in July 2002 and July 2003 to collect pollen at various heights within the boundary layer. Measurements of pollen concentration and viability were taken for pollen that was collected at a variety of heights through and above the atmospheric boundary layer. They observed that pollen concentration dropped off quickly just above the surface, but was nearly constant throughout the rest of the boundary layer (Figure 3.13). Some pollen was observed to escape the boundary layer. Pollen viability was measured to drop off exponentially with height, but pollen near the top of the atmosphere still retained a small percentage of viability (Figure 3.13).

Modeled profiles of pollen concentration are produced for three times through the course of the day in Figure 3.14. In order to keep track of pollen that left the model domain, periodic boundary conditions were imposed on the pollen, so that pollen leaving the domain on one side would re-enter the domian on the opposite side. During the early portion of the day, the amount of pollen in the atmosphere decreases quickly with height, and does not settle at a lower boundary to match the plots of B01. However, later in the afternoon when more pollen has been released, a constant amount of pollen is mixed through the upper third of the boundary layer. The LDM model does not take into account the possibility of released pollen being advected into the domain, which may contribute to some of the differences between B01 and our study.

Profiles of average pollen viability through the boundary layer are shown in Figure 3.15. Average pollen viability near the surface remains consistently high throughout the day, which is a result of the fresh pollen being continually produced at that level, with the peak in viability occurring slightly above the ground at the level of pollen release. At the beginning of the day, the averaged profile retains its

viability quite well with height. This should not be surprising since temperatures are still cooler and the boundary layer is only a few hundred meters deep. Later in the day the average viability with height decreases more quickly with respect to boundary layer height. This results from a combination of warmer conditions in the afternoon which promote more rapid water loss as well as the inclusion of pollen that has been exposed to the atmosphere for longer periods of time in the averaging. Pollen viability through most of the boundary layer is predicted to be greater than was measured by B01, but matches near the top of the boundary layer in the afternoon.

3.4 Conclusions

The ARPS/LDM model has been used to simulate the movement and deposition of pollen from a source field. The model was compared to a previous version of the LDM using limited input to generate its predictions and to observations taken from a 2003 field study. The ARPS/LDM also made predictions of the viability of deposited pollen to examine the potential for outcross between GM maize and conventionally grown maize. Comparisons were also made to a separate field study reported by B01 to measure vertical profiles of the aerial concentration and average viability of pollen.

The ARPS/LDM model captured the main features of pollen deposition. The largest concentration of pollen was over and around the source field, with a deposition plume directed away from the source field in the direction. Both versions of the LDM overpredicted pollen deposition at most points where observation were taken, with the ARPS/LDM giving higher values of deposition between the two. Near field deposition was overpredicted by the models, but is thought to be due to the increased height of pollen release rather than model errors. Both models predicted that pollen could be transported over distances of at least a few kilometers.

The predicted values of viability for deposited pollen by the ARPS/LDM suggests that pollen transported at least five kilometers may still be at risk to pollinate receptor plants. On moderately windy days as were modeled, the potential for outcrossing may extend up to 10-15 kilometers. While the low concentration of pollen will make it difficult for transported pollen to outcompete local pollen, it must still be considered a potential threat to the purity of the receptor plants.

From examining the vertical profiles, it is evident that pollen is being distributed through the boundary layer early in the day and some value of concentration is being maintained throughout the day. Although the shape of the plots differed from the data given by B01, it still implies that large amounts of pollen can be moved long distances. The predicted values of pollen viability from the ARPS/LDM are much higher than the data from B01, and supports the idea of long-distance transport of viable pollen.

Confirmation of viable pollen being transported over kilometers would be an invaluable piece of information to assess the potential risks of cross-pollination. Most current field projects only look at outcross potential over a few hundred meters, and conclude that cross-pollination beyond that distance rarely or never occurs. This effect may be linked to the decrease in pollen concentration rather than viability, meaning that the risk of cross-pollination may be a function of the concentration of viable pollen.

3.5 References

Aylor, D. E., 2002: Settling speed of corn (*Zea mays*) pollen. *J. Aerosol Sci.,* **33**, 1601-1607.

Aylor, D. E., 2003: Rate of dehydration of corn (Zea mays) pollen. *J. Exp. Bot.,* **54**, 2307-2313.

Aylor D. E., 2004: Survival of maize (Zea mays) pollen exposed in the atmosphere. *Agric. For. Meteor.,* **123**, 125-133.

Aylor, D. E., Schultes N. P., Shields E. J., 2003: An aerobiological framework for assessing cross-pollination in maize. *Agric. For. Meteor.,* **119**, 111-129.

Barnabus, B., 1985: Effect of water loss on germination ability of maize (*Zea mays* L.) Pollen. *Annals of Botany.,* **55**, 201-204.

Bassetti, P., and M. E. Westgate, 1993: Senescence and receptivity of maize silks. *Crop Sci.,* **33**, 275-278.

Bassetti, P., and M. E. Westgate, 1993: Water deficit affects receptivity of maize silks. *Crop Sci.,* **33**, 279-282.

Brunet, Y., X. Foueillassar, A. Audran, D. Garrigou, and S. Dayau, 2004: Evidence for long-range transport of viable maize pollen. *Extended Abstracts, 16th Conf. Biometeorology and Aerobiology*, Vancouver, BC, Amer. Meteor. Soc., CD-ROM, 4A.2.

Bullock J. M., and R. T. Clarke, 2000: Long distance seed dispersal by wind: measuring and modelling the tail of the curve. *Oceologia,* **124**, 506-521.

Chow, F. K., A. P. Weigel, R. L. Street, M. W. Rotach, and M. Xue, 2006: High-resolution large-eddy simulations of flow in a steep Alpine valley. Part I: Methodology, verification, and sensitivity studies. *J. Appl. Meteor.,* **45**, 63-86.

Arritt, R. W., C. A. Clark, A. S. Goggi, H. Lopez Sanchez, M. E. Westgate and J. M. Riese, 2007: Lagrangian numerical simulations of canopy air flow effects on maize pollen dispersal. *Field Crops Research* (in press).

Deardorff, J. W., 1972: Numerical investigation of a neutral and unstable planetary boundary layers. *J. Atmos. Sci.*, **29**, 91-115.

Dupont, S., V. d'Ornon, and Y. Brunet, 2006: Large-eddy simulation of forest edge flow with ARPS. *27th Conf. on Ag. For. Meteor.,* San Diego, CA, Amer. Meteor. Soc., CD-ROM, JP2.2.

Emberlin, J., B. Adams-Groom, and J. Tidmarsh, 1999: A report on the dispersal of maize pollen. National Pollen Research Unit, University College Worcester, UK.

Fonseca, A. E., and M. E. Westgate, 2005: Relationship between dessication and viability of maize pollen. *Field Crop Res.,* **94**, 114-125.

Hansen-Jesse, L. C., J. J. Obrycki, 2000: Field deposition of Bt transgenic corn pollen: lethal effects on the monarch butterfly. *Oecologia,* **125**, 241-248.

Klein, E. K., C. Lavigne, X. Foueillassar, P.-H. Gouyon, and C. Laredo, 2003: Corn pollen dispersal: quasi-mechanistic model and field experiments. *Ecol. Monogr.,* **73**, 131-150.

Kerhoas, C., G. Gay, and C. Dumas, 1987: A multidisciplinary approach to the study of the plasma membrane of *Zea mays* pollen during controlled dehydration. *Planta,* **171**, 1-10.

Lincoln, R. J., G. A. Boxshall, P. F. Clark, 1982: *A dictionary of ecology, evolution and systematics.* Cambridge University Press, 371 pp.

Lohnquist, J. H., and R. W. Jugenheimer, 1943: Factors affecting the success of pollination in corn. *J. Amer. Soc. Agron.,* **35**, 923-933.

Luna, V. S., J. M. Figueroa, M. B. Baltazar, L. R. Gomez, R. Townsend, and J. B. Schoper, 2001: Maize pollen longevity and distance isolation requirement for effective pollen control. *Crop Sci.,* **41**, 1551-1557.

Ma, B. L., K. D. Subedi, and L. M. Reid, 2004: Extent of cross-fertilization in maize by pollen from neighboring transgenic hybrids. *Crop Sci.,* **44**, 1273-1282.

Moeng, C. H., and J. C. Wyngaard, 1989: Evaluation of turbulent transport and dissipation closures in second-order modeling. *J. Atmos. Sci.*, **46**, 2311-2330.

Nap, J.-P., P. L. J. Metz, M. Escaler, and A. J. Conner, 2003: The release of genetically modified crops into the environment. Part I: Overview of current status and regulations. *The Plant Journal,* **33**, 1-18.

Peterson, D. F., 1942: Duration of receptiveness in corn silks. *Jour. Amer. Soc. Agron.,* **34**, 369-372.

Roeckel-Drevet, P., C. Digonnet, E. Matthys-Rochon, D. Champiat, and C. Dumas, 1995: Fertility of *Zea mays* pollen during dehydration: Physiological steps outlined by nucleotide measurements. *Plant Physiol. Biochem.,* **33**, 289-294.

Schoper, J. B., R. J. Lambert, and B. L. Vasilas, 1987: Pollen viability, pollen shedding, and combining ability for tassel heat tolerance in maize. *Crop Sci.,* **27**, 27-31.

Uribelarrea, M., J. Carcova, M. E. Otegui, and M. E. Westgate, 2002: Pollen production, pollination dynamics, and kernel set in maize. *Crop Sci.* **42**, 1910-1918.

Wilson, J. C., B. G. Lafleur, H. Hilvert, W. R. Seebaugh, J. Fox, C. A. Brock, B. Huebert, D. R. Geseler, J. Mullen, and J. M. Reeves, 2004: Function and performance of a low turbulence inlet fo sampling super-micron particles from aircraft platforms. *Aerosol Sci. Tech.,* **38**, 790-802.

Xue, M., K. K. Droegemeier, and V. Wong, 2000: The Advanced Regional Prediction System (ARPS) - A multiscale nonhydrostatic atmospheric simulation and reiction tool. Part I: Model dynamics and verification. *Meteor. Atmos. Phys.,* **75**, 161-193.

Xue, M., K. K. Droegemeier, V. Wong, A. Shapiro, K. Brewster, F. Carr, D. Weber, Y. Liu, and D.-H. Wang,2001: The Advanced Regional Prediction System (ARPS) - A multiscale nonhydrostatic atmospheric simulation and prediction tool. Part II: Model physics and applications. *Meteor. Atmos. Phys.,* **76**, 134-165. 3.15

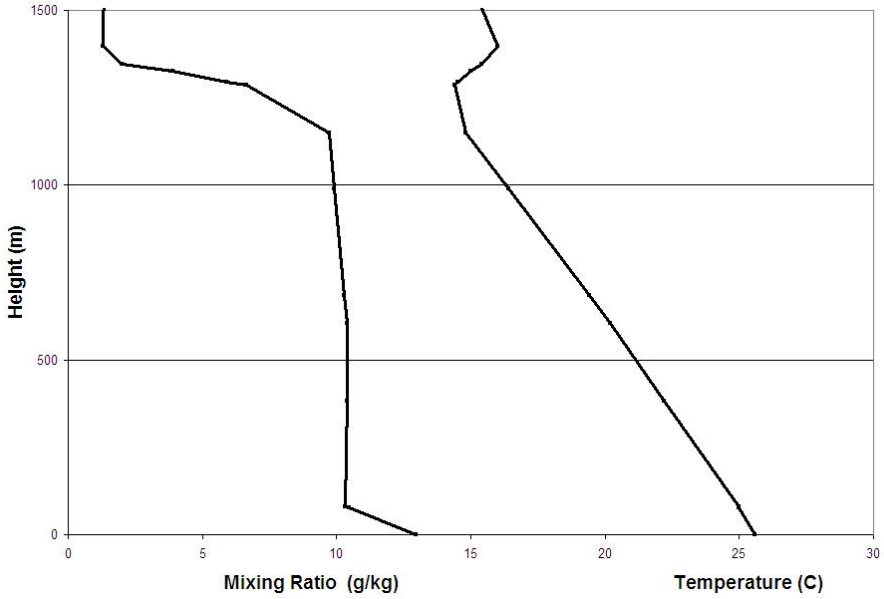
1500
1000
500
0
Height (m)
0
5
10
15
20
25
30
Mixing Ratio (g/kg)
Temperature (C)

(a)

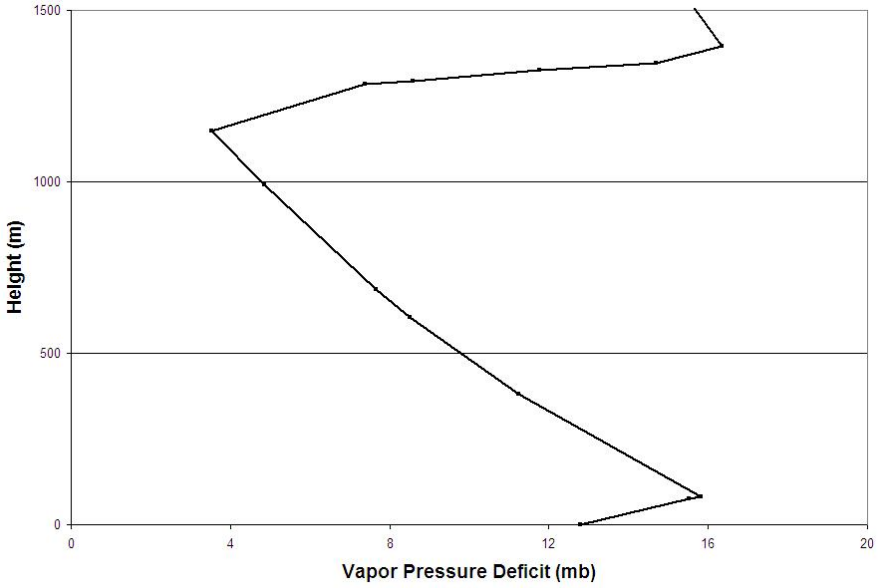
1500
1000
500
0
Height (m)
0
4
8
12
16
20
Vapor Pressure Deficit (mb)

(b)

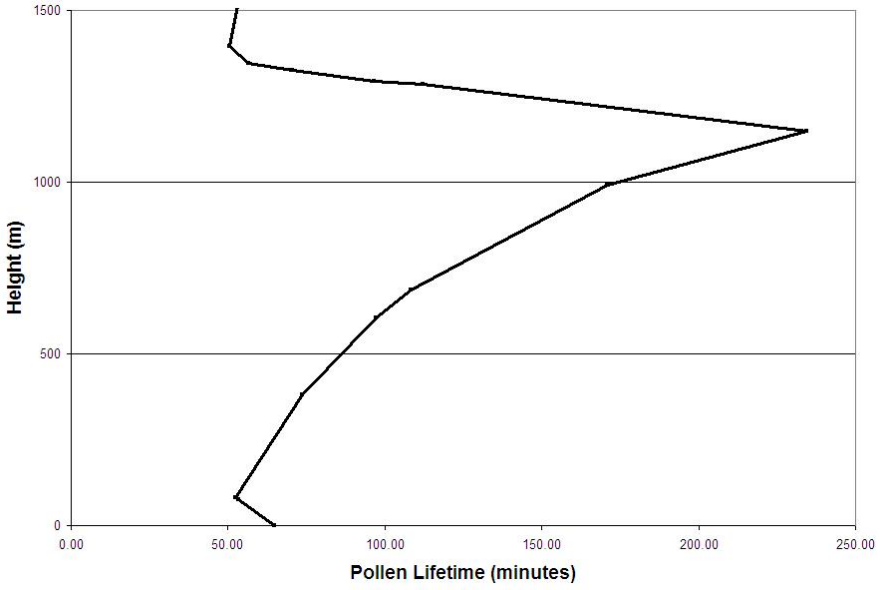

(c)

Figure 3.1 Representative summer sounding showing vertical profiles of temperature and mixing ration (a), vapor pressure deficit (b), and estimated pollen lifetime (c). The sounding was taken from Davenport, IA.

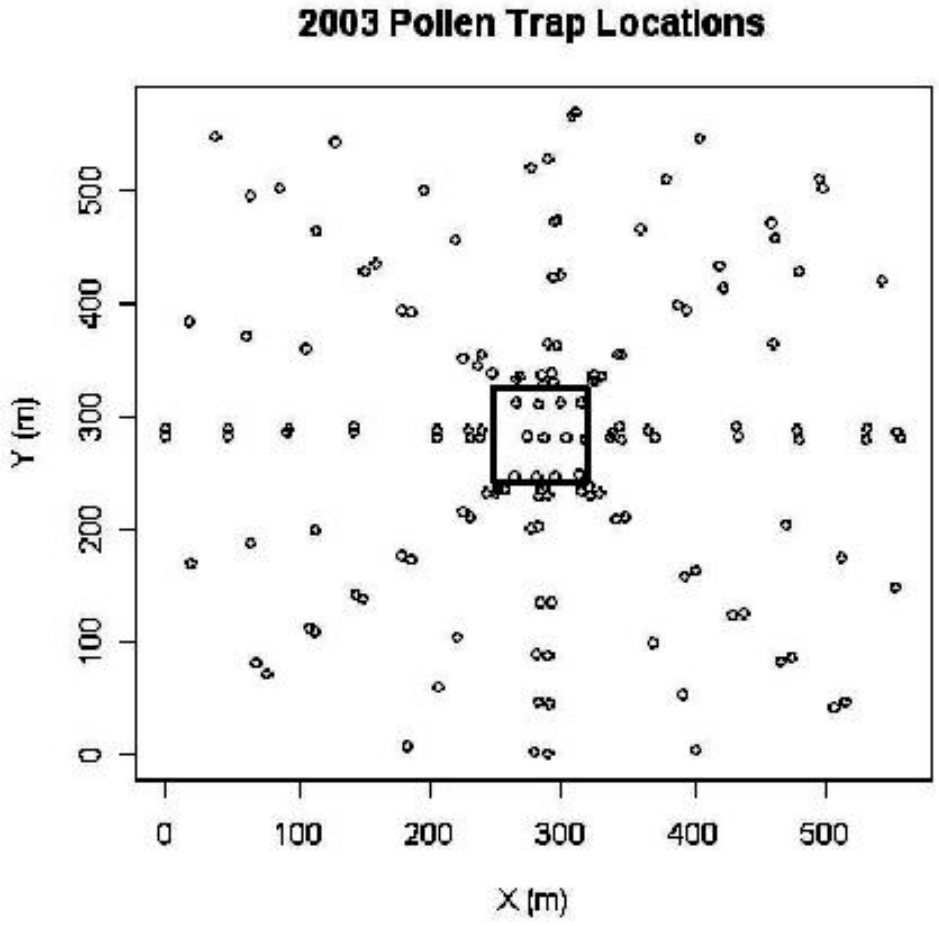

Figure 3.2 Distribution of pollen traps around and within the source field. The small square notes the boundaries of the source field.

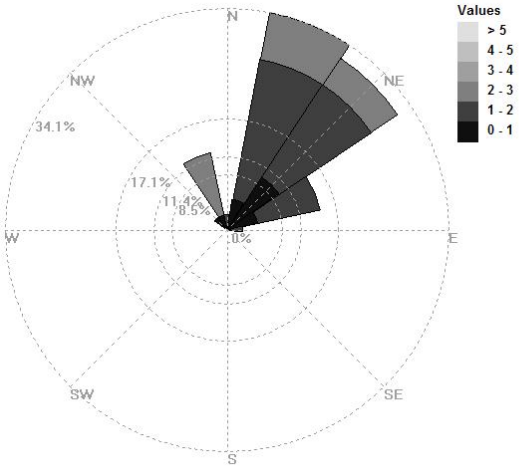
Values
> 5
4 - 5
3 - 4
2 - 3
1 - 2
0 - 1
N
NE
E
SE
S
SW
W
NW
34.1%
17.1%
11.4%
8.5%
0%

(a)

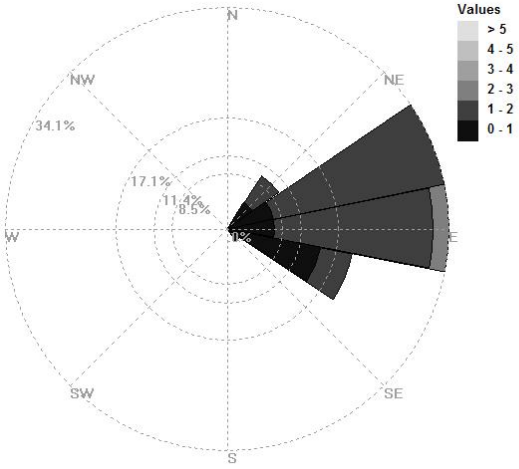
Values
> 5
4 - 5
3 - 4
2 - 3
1 - 2
0 - 1
N
NE
E
SE
S
SW
W
NW
34.1%
17.1%
11.4%
8.5%
1%

(b)

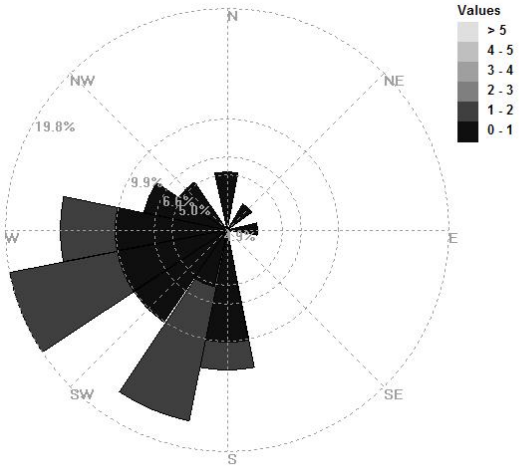

(c)

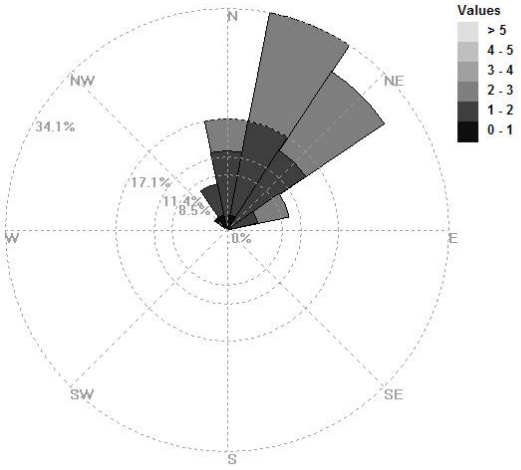

(d)

Figure 3.3 Observed wind data for Aug. 8 (a), Aug. 9 (b), Aug. 10 (c),and Aug. 11 (d).

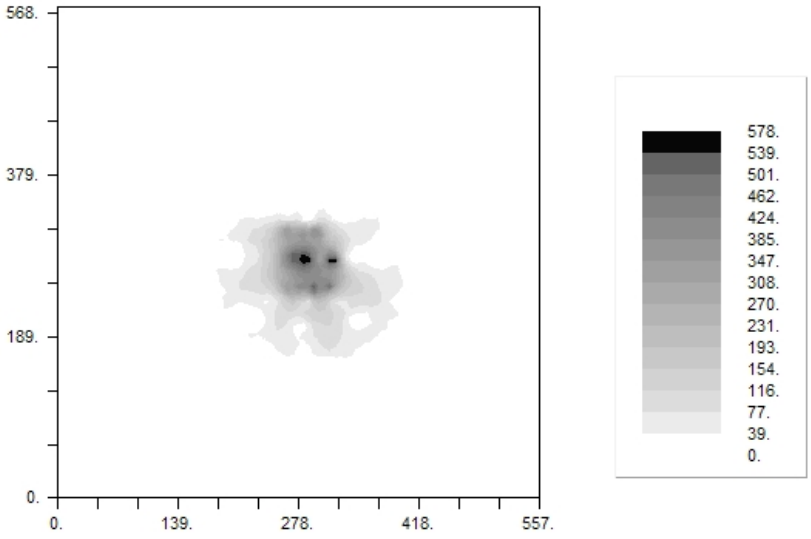
568.
379.
189.
0.
0.
139.
278.
418.
557.
578.
539.
501.
462.
424.
385.
347.
308.
270.
231.
193.
154.
116.
77.
39.
0.

(a)

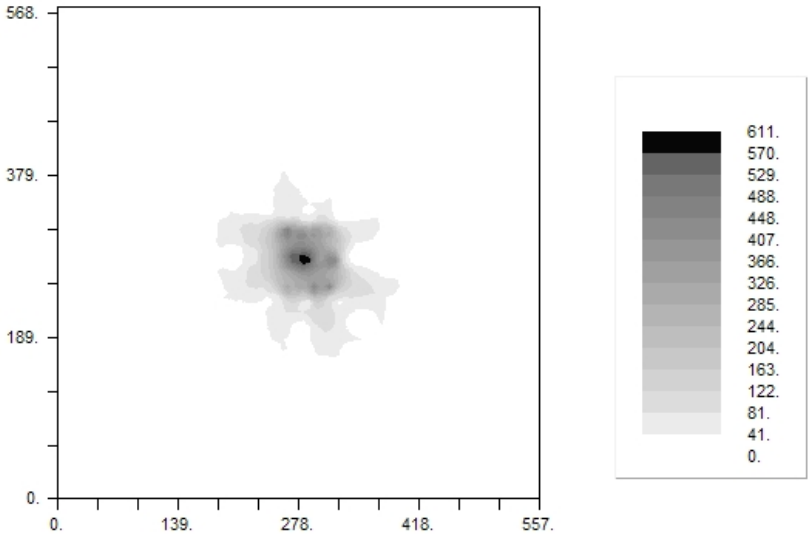
568.
379.
189.
0.
0.
139.
278.
418.
557.
611.
570.
529.
488.
448.
407.
366.
326.
285.
244.
204.
163.
122.
81.
41.
0.

(b)

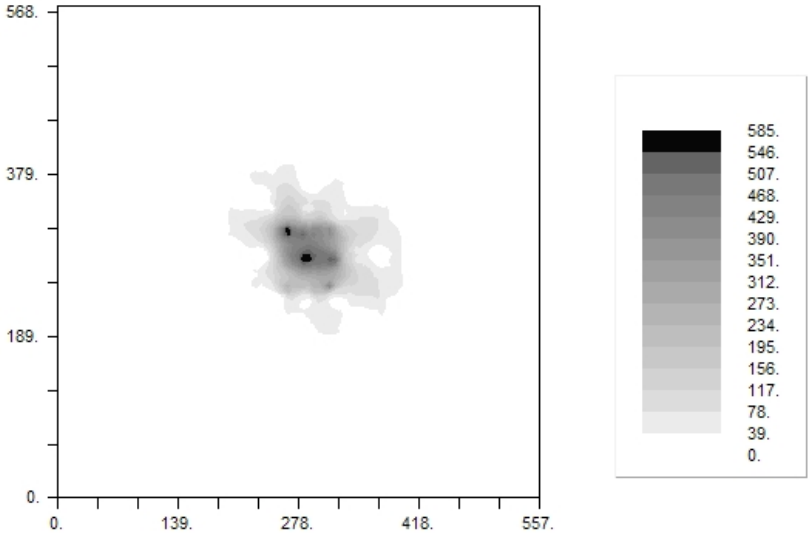

(c)

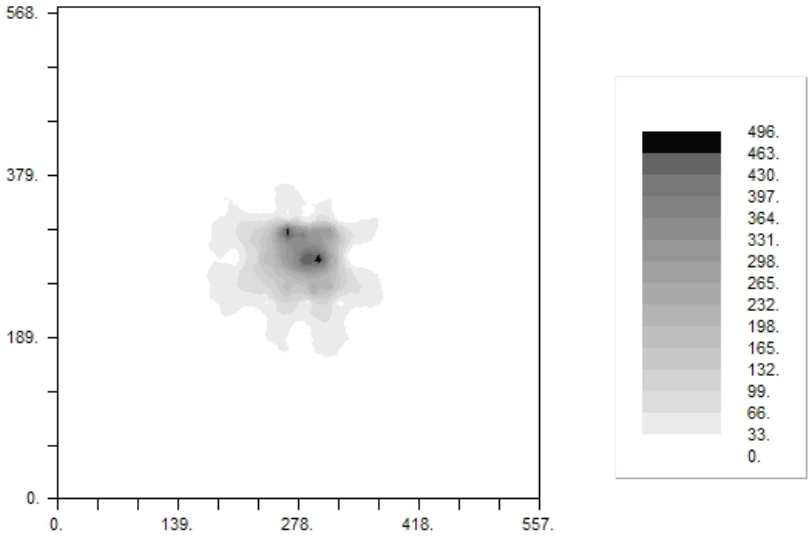

(d)

Figure 3.4 Interpolated deposition patterns from field observations(in grains m^{-2}) for Aug. 8 (a), Aug. 9 (b), Aug. 10 (c), and Aug. 11 (d).

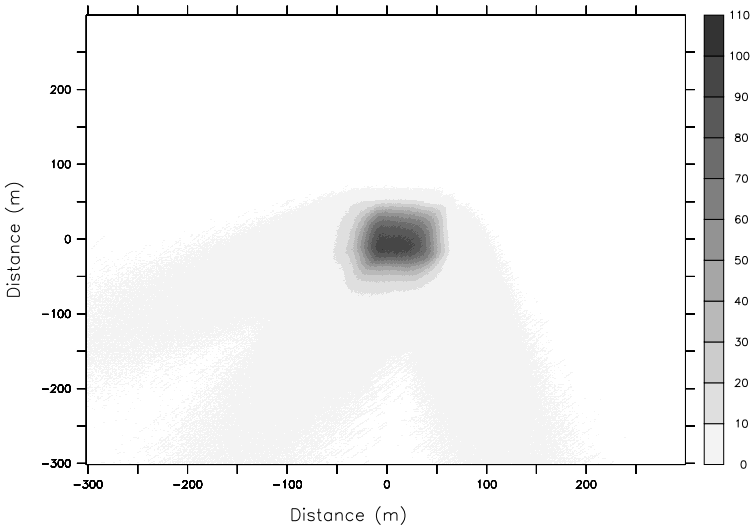
Distance (m)
Distance (m)
200
100
0
−100
−200
−300
−300
−200
−100
0
100
200
110
100
90
80
70
60
50
40
30
20
10
0

(a)

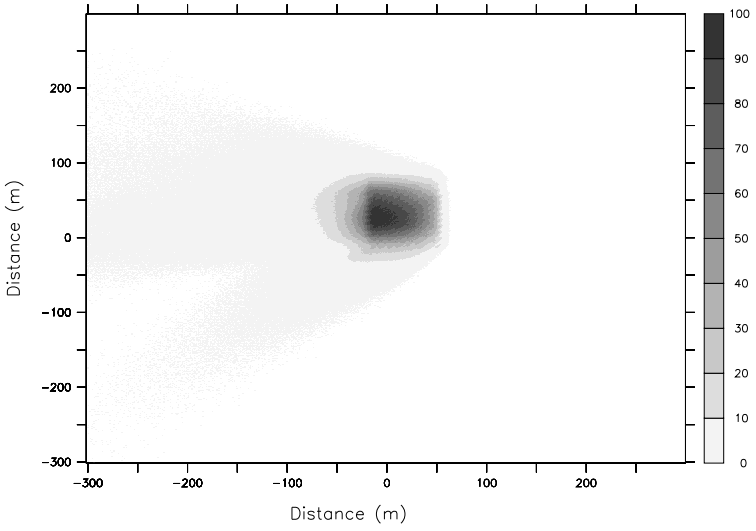
Distance (m)
Distance (m)
200
100
0
−100
−200
−300
−300
−200
−100
0
100
200
100
90
80
70
60
50
40
30
20
10
0

(b)

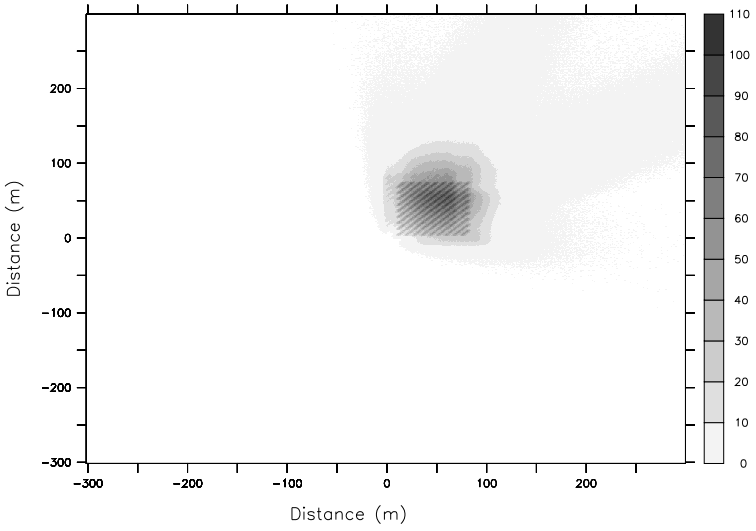

(c)

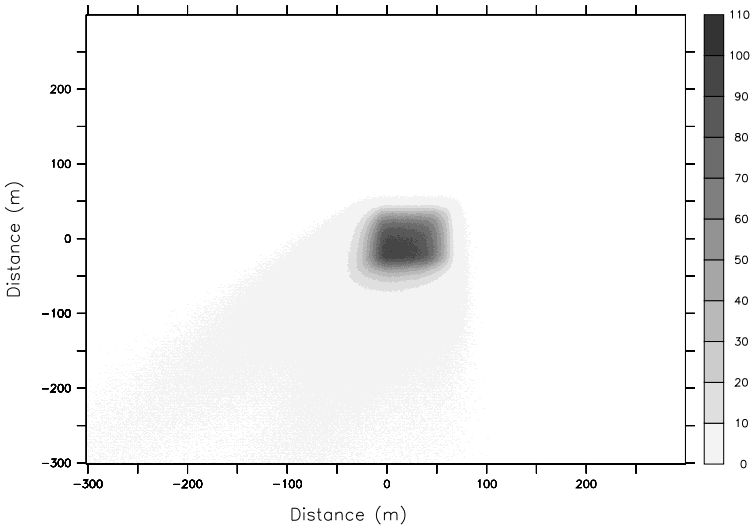

(d)

Figure 3.5 Near-field pollen deposition as predicted by the Pre/LDM (in grains m^{-2}) for Aug. 8 (a), Aug. 9 (b), Aug. 10 (c), and Aug. 11 (d).

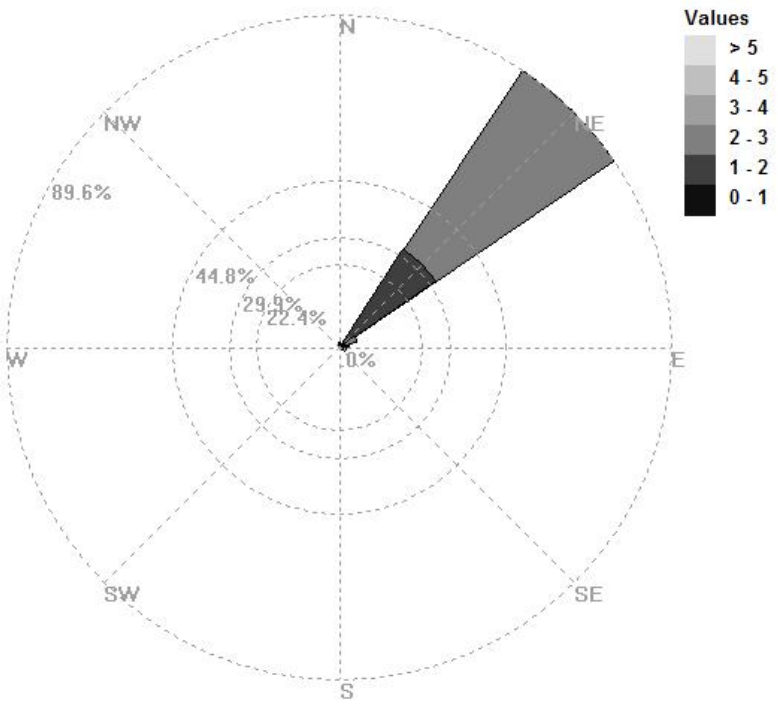
Values
> 5
4 - 5
3 - 4
2 - 3
1 - 2
0 - 1
N
NE
E
SE
S
SW
W
NW
89.6%
44.8%
29.9%
22.4%
0%

(a)

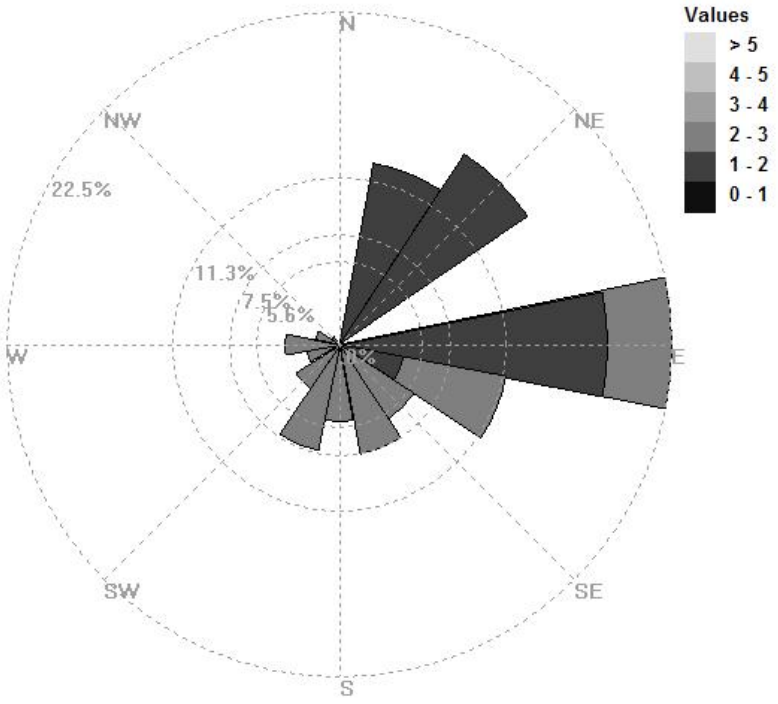
Values
> 5
4 - 5
3 - 4
2 - 3
1 - 2
0 - 1
N
NE
E
SE
S
SW
W
NW
22.5%
11.3%
7.5%
5.6%
0%

(b)

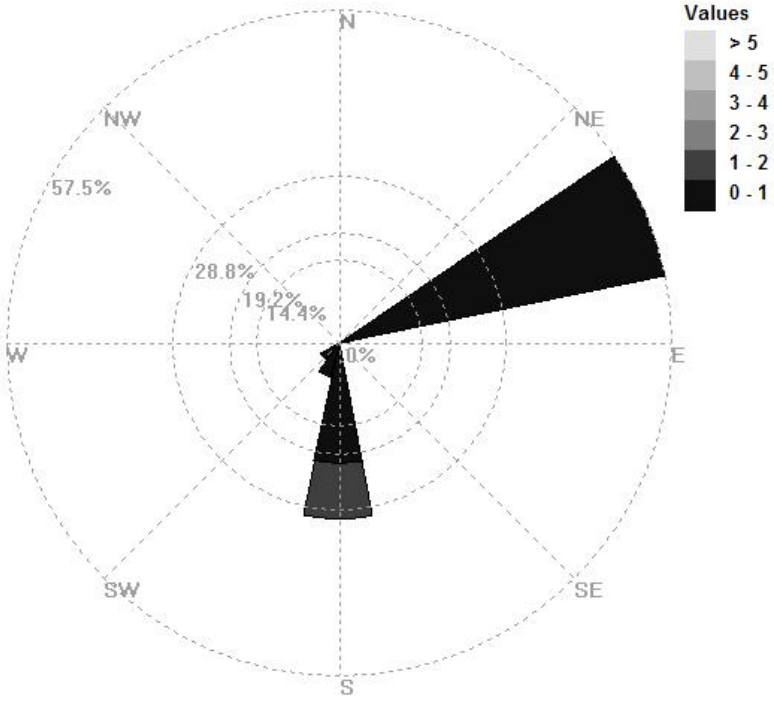

(c)

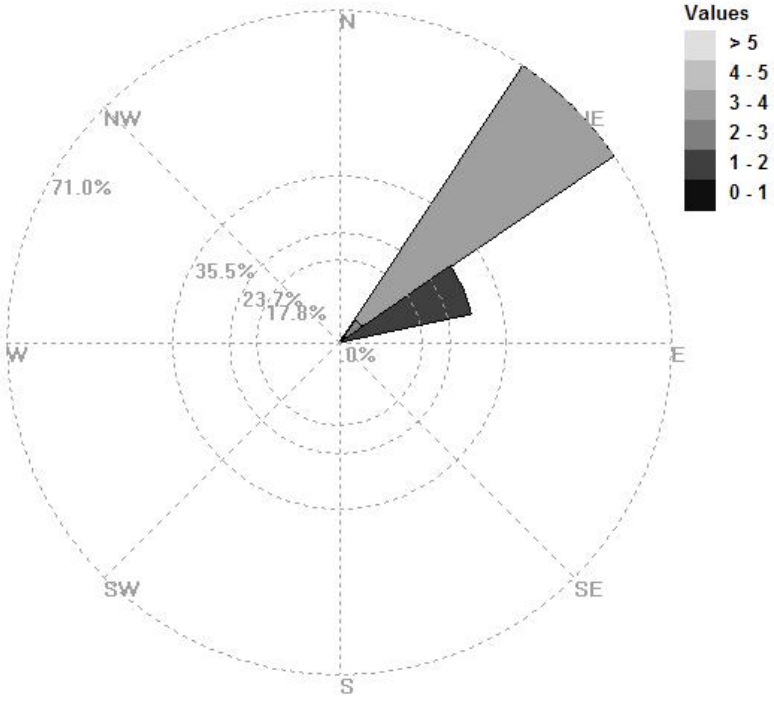

(d)

Figure 3.6 Modeled wind data for Aug. 8 (a), Aug. 9 (b), Aug. 10 (c), and Aug. 11 (d).

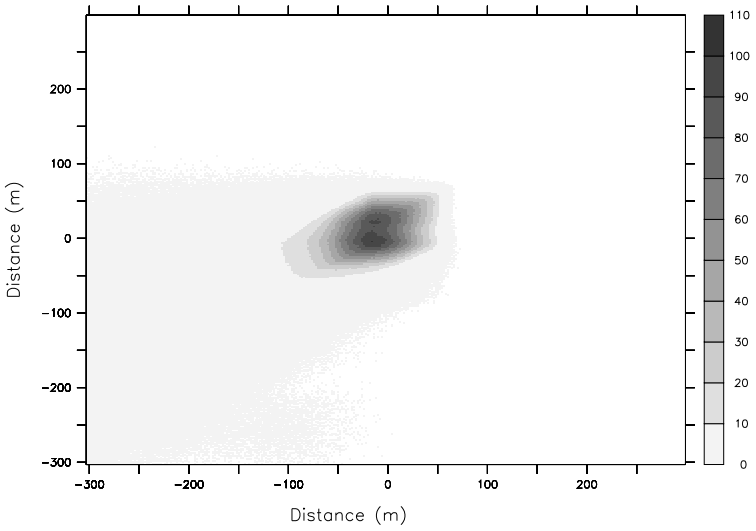
Distance (m)
200
100
0
−100
−200
−300
−300
−200
−100
0
100
200
Distance (m)
110
100
90
80
70
60
50
40
30
20
10
0

(a)

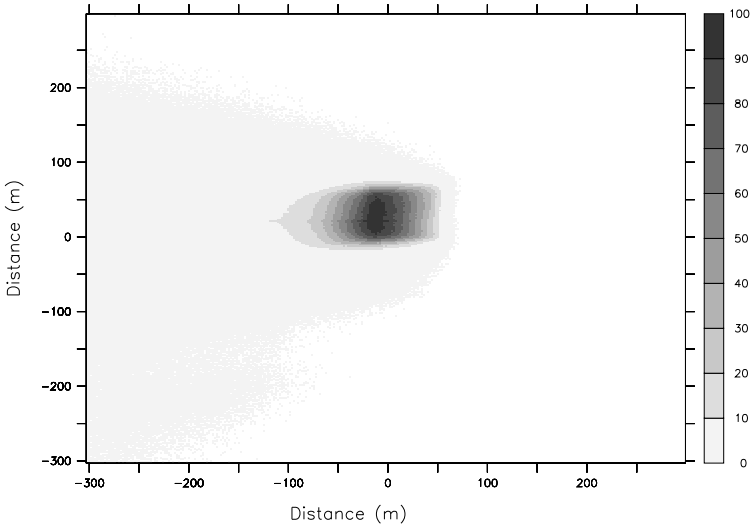
Distance (m)
200
100
0
−100
−200
−300
−300
−200
−100
0
100
200
Distance (m)
100
90
80
70
60
50
40
30
20
10
0

(b)

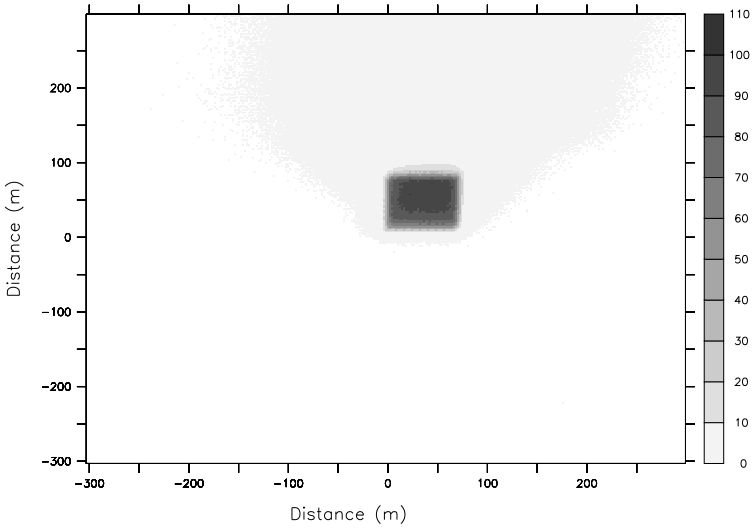

(c)

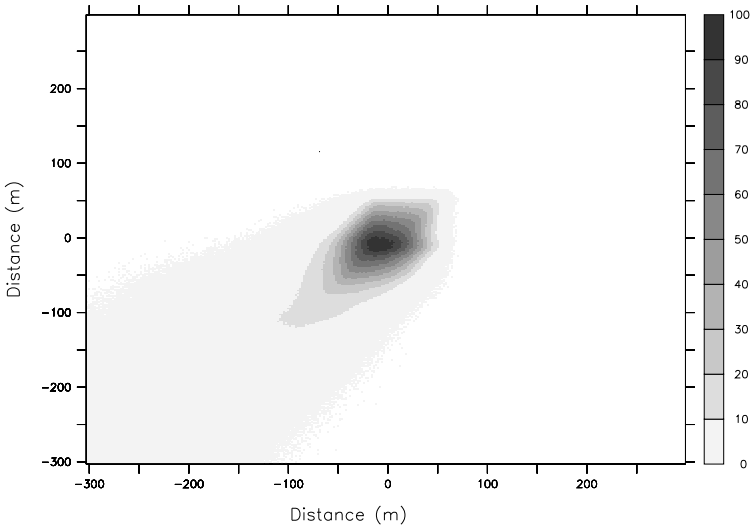

(d)

Figure 3.7 Near-field pollen deposition as predicted by the ARPS/LDM (in grains m^{-2}) for Aug. 8 (a), Aug. 9 (b), Aug. 10 (c), and Aug. 11 (d).

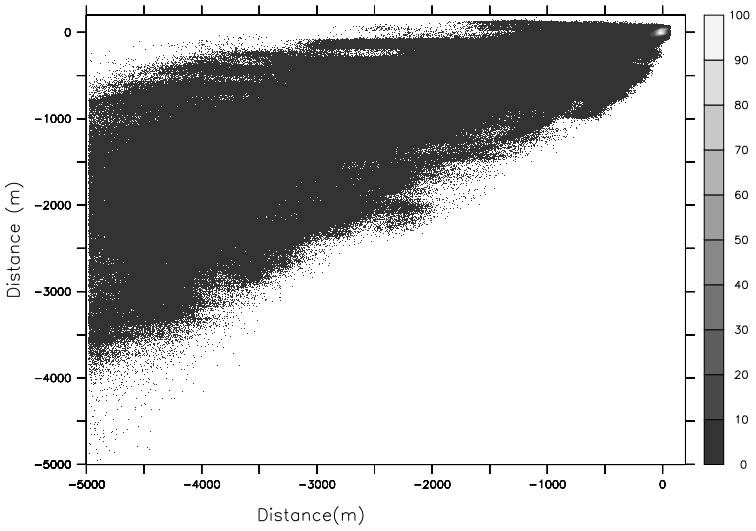
Distance (m)
Distance(m)
0
−1000
−2000
−3000
−4000
−5000
−5000
−4000
−3000
−2000
−1000
0
100
90
80
70
60
50
40
30
20
10
0

(a)

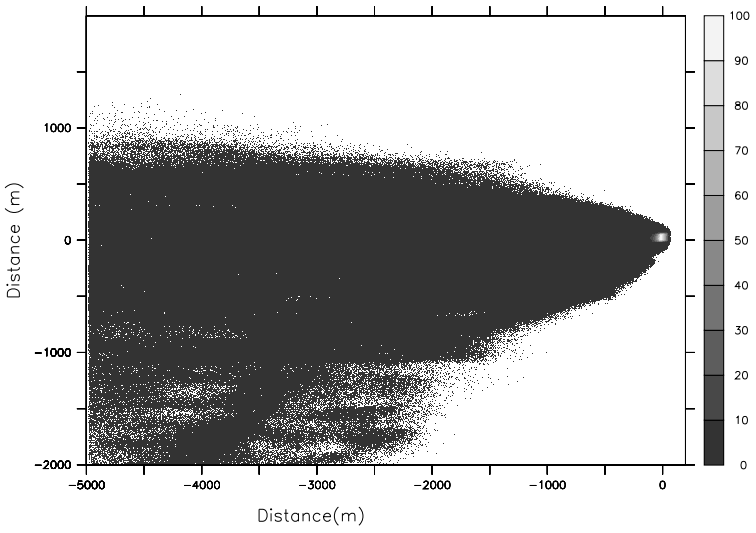
Distance (m)
Distance(m)
1000
0
−1000
−2000
−5000
−4000
−3000
−2000
−1000
0
100
90
80
70
60
50
40
30
20
10
0

(b)

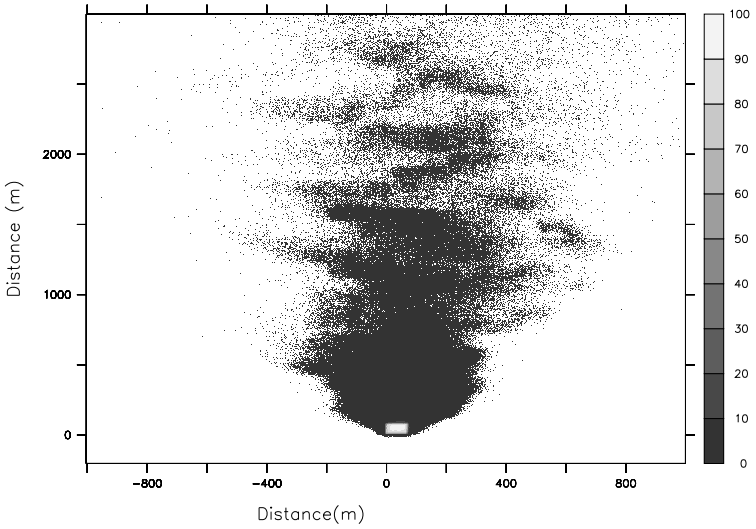

(c)

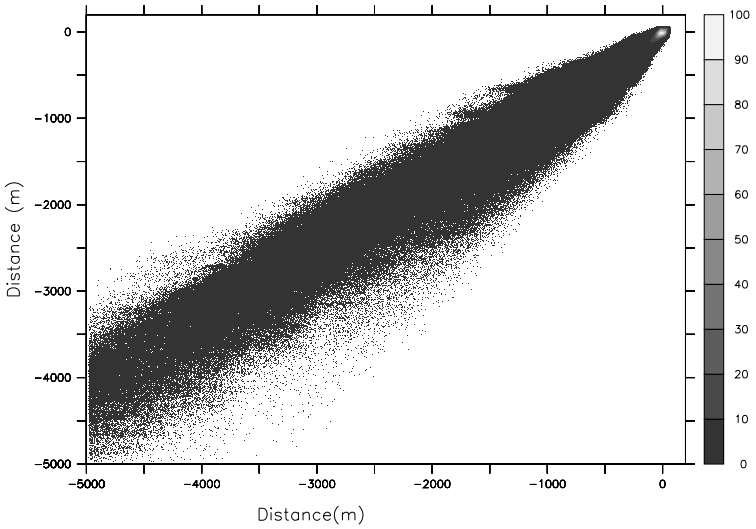

(d)

Figure 3.8 Far-field pollen deposition as predicted by the ARPS/LDM (in grains m^{-2}) for Aug. 8 (a), Aug. 9 (b), Aug. 10 (c), and Aug. 11 (d).

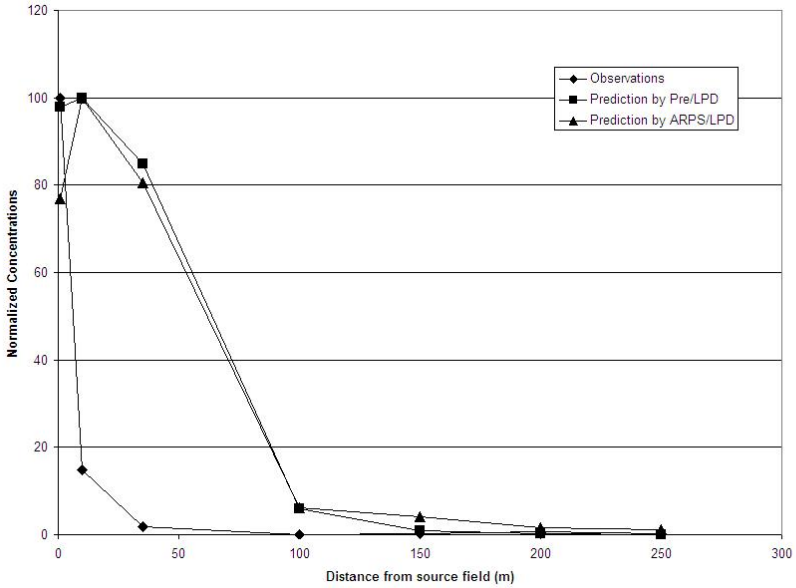
Observations
Prediction by Pre/LPD
Prediction by ARPS/LPD
Normalized Concentrations
Distance from source field (m)
0
20
40
60
80
100
120
0
50
100
150
200
250
300

(a)

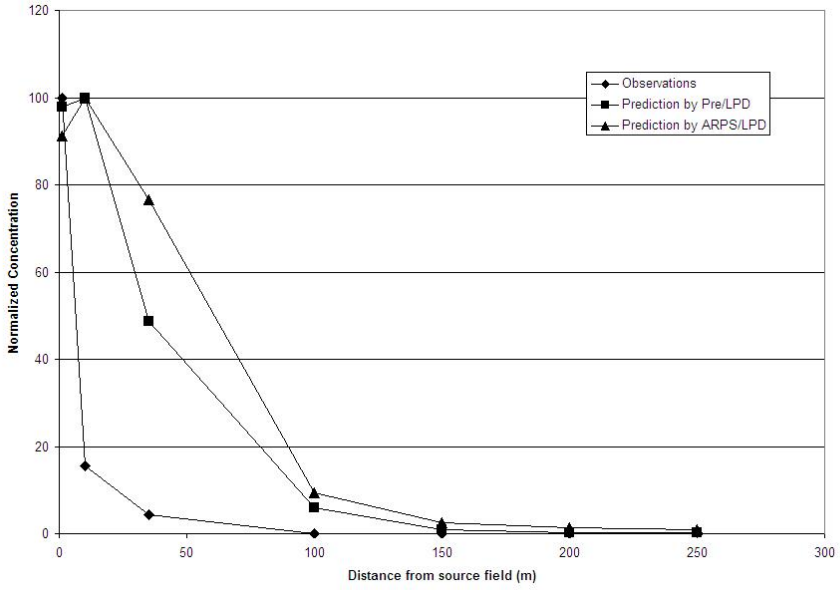
Observations
Prediction by Pre/LPD
Prediction by ARPS/LPD
Normalized Concentration
Distance from source field (m)
0
20
40
60
80
100
120
0
50
100
150
200
250
300

(b)

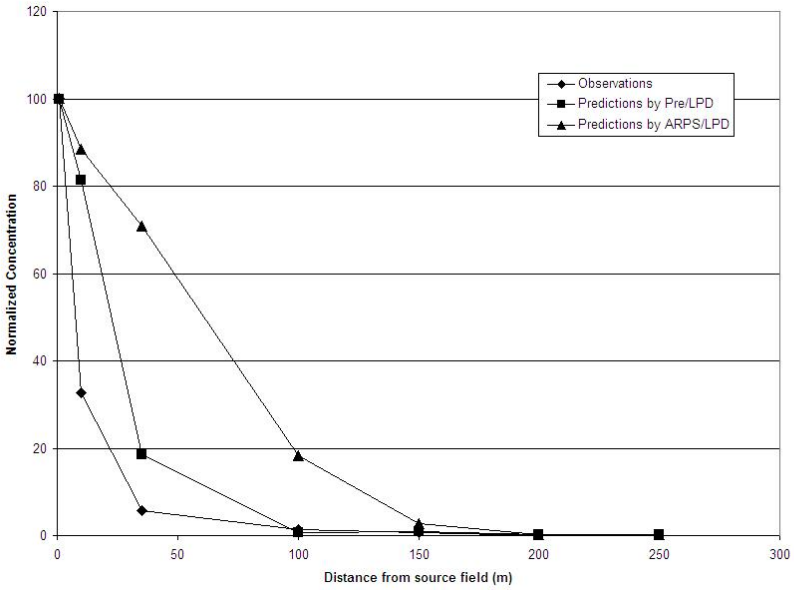

(c)

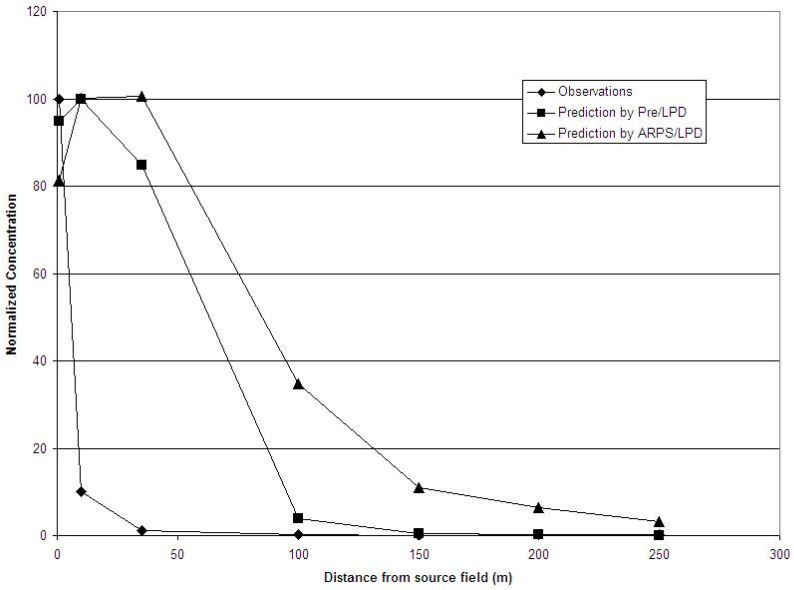

(d)

Figure 3.9 Comparison of the modeled results to the observations along the primary direction of pollen dispersion for Aug. 8 (a), Aug. 9 (b), Aug. 10 (c), and Aug. 11 (d).

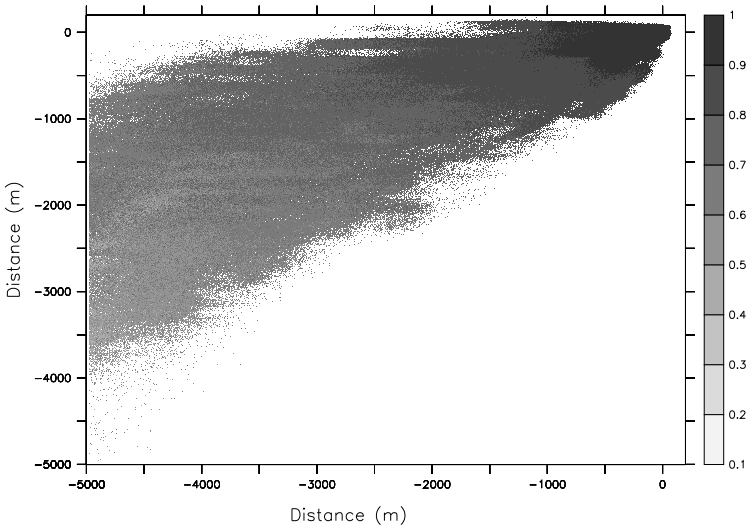
0
−1000
−2000
−3000
−4000
−5000
Distance (m)
−5000
−4000
−3000
−2000
−1000
0
Distance (m)
1
0.9
0.8
0.7
0.6
0.5
0.4
0.3
0.2
0.1

(a)

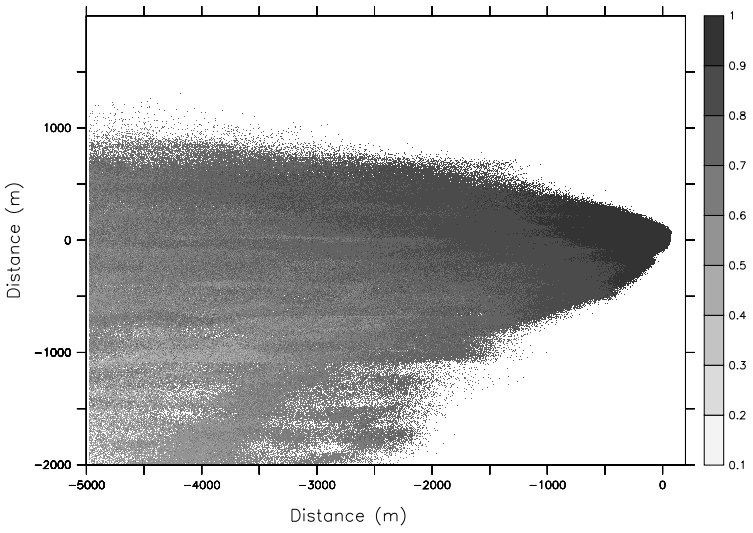
1000
0
−1000
−2000
Distance (m)
−5000
−4000
−3000
−2000
−1000
0
Distance (m)
1
0.9
0.8
0.7
0.6
0.5
0.4
0.3
0.2
0.1

(b)

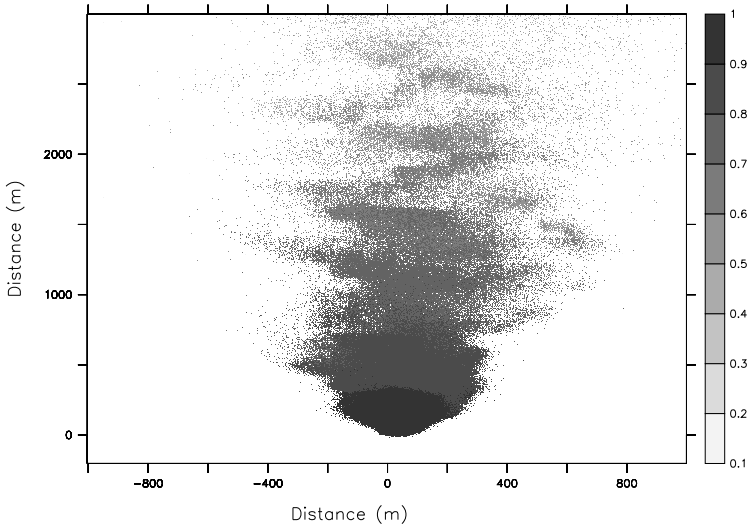

(c)

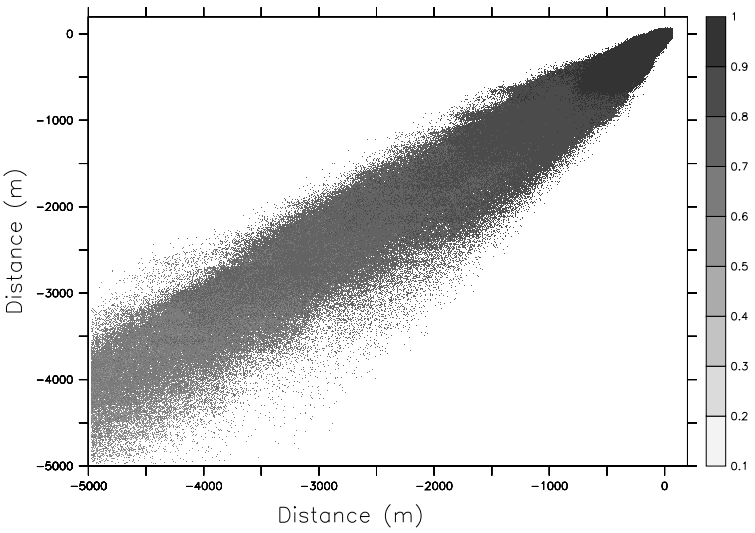

(d)

Figure 3.10 Average pollen viability upon deposition (in % viable) for Aug. 8 (a), Aug. 9 (b), Aug. 10 (c), and Aug. 11 (d).

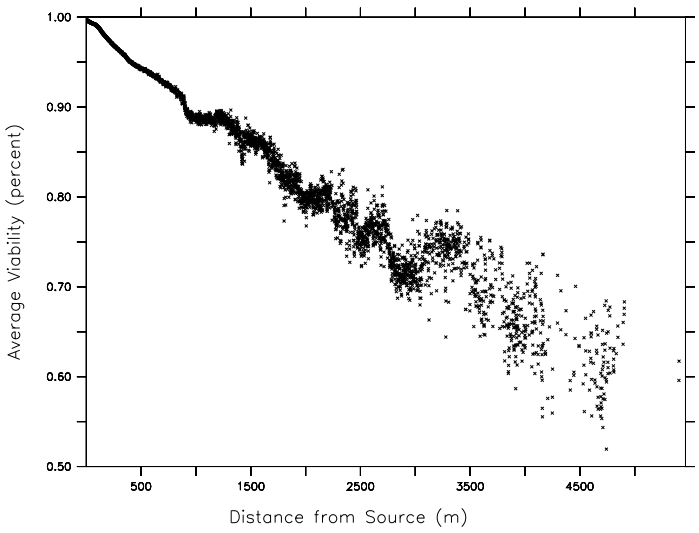
1.00
0.90
0.80
0.70
0.60
0.50
Average Viability (percent)
500
1500
2500
3500
4500
Distance from Source (m)

(a)

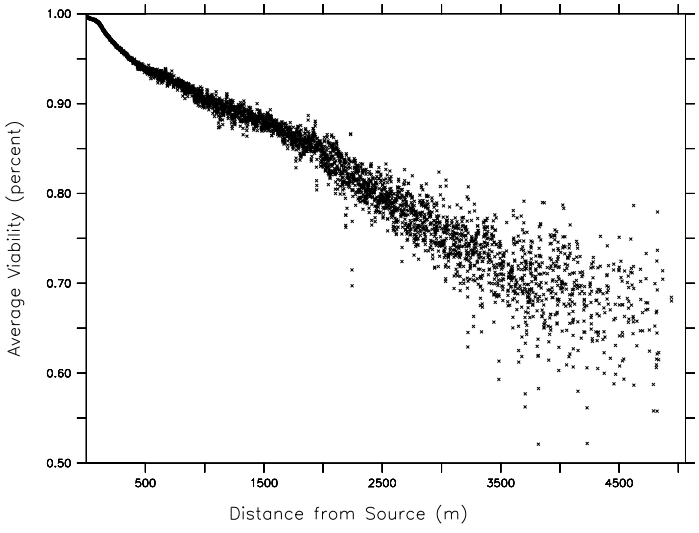
1.00
0.90
0.80
0.70
0.60
0.50
Average Viability (percent)
500
1500
2500
3500
4500
Distance from Source (m)

(b)

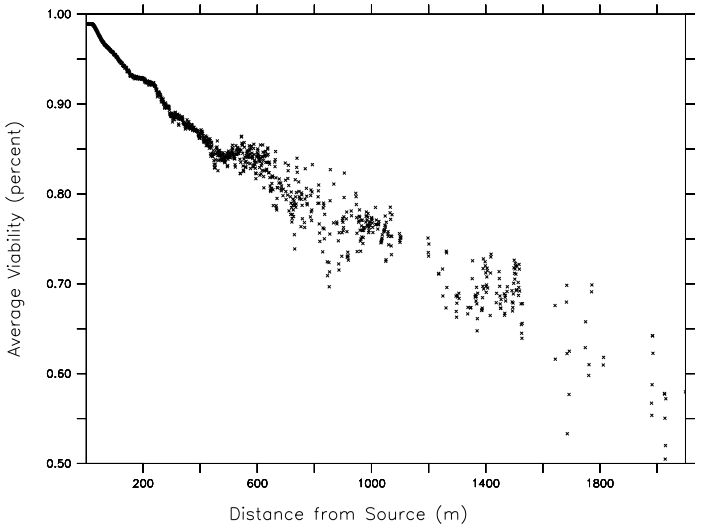

(c)

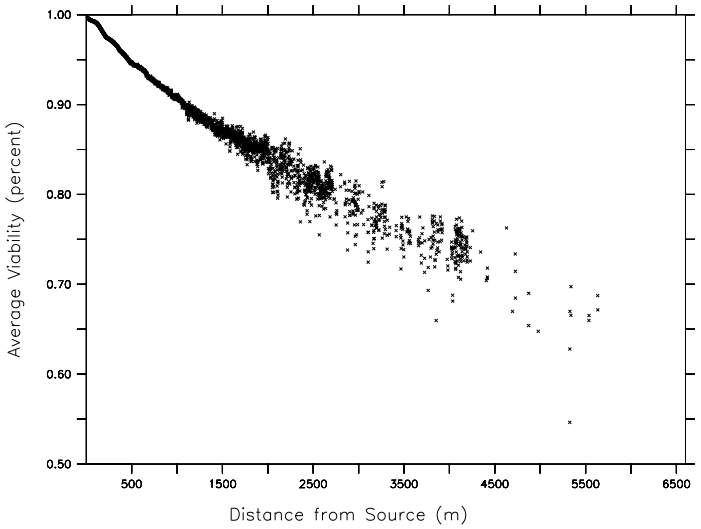

(d)

Figure 3.11 Transects of pollen viability upon deposition in the direction of main pollen shed on each day (in % viable) for Aug. 8 (a), Aug. 9 (b), Aug. 10 (c), and Aug. 11 (d).

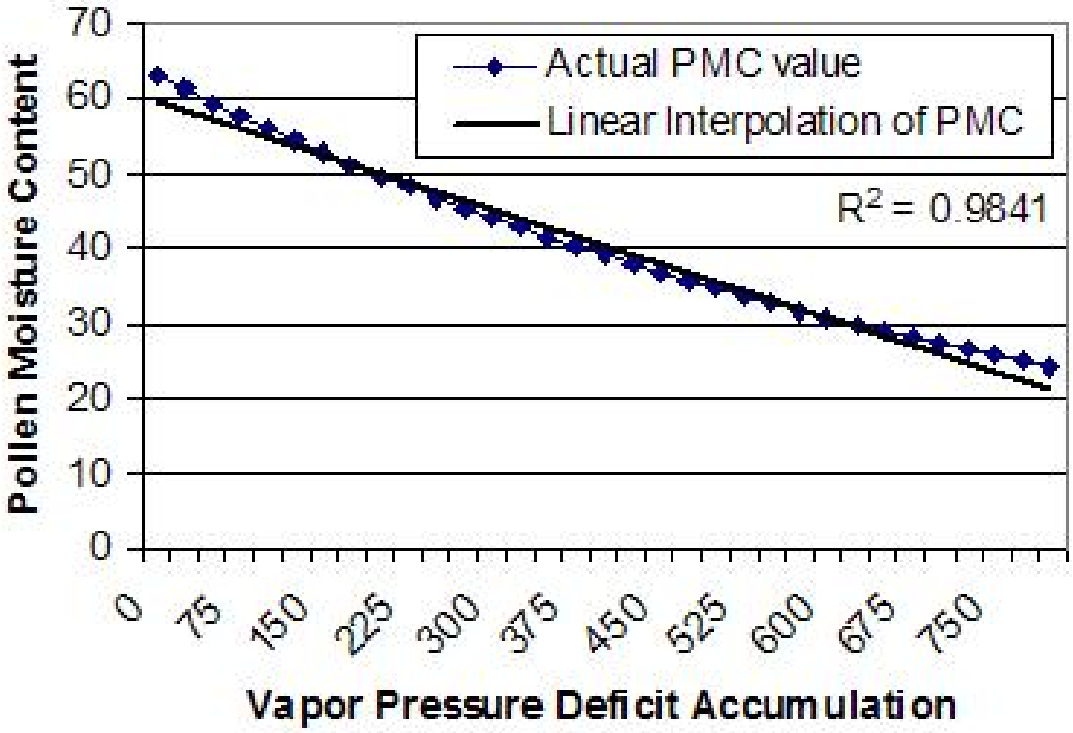

Figure 3.12 Linear approximation of the exponential curve representing PMC.

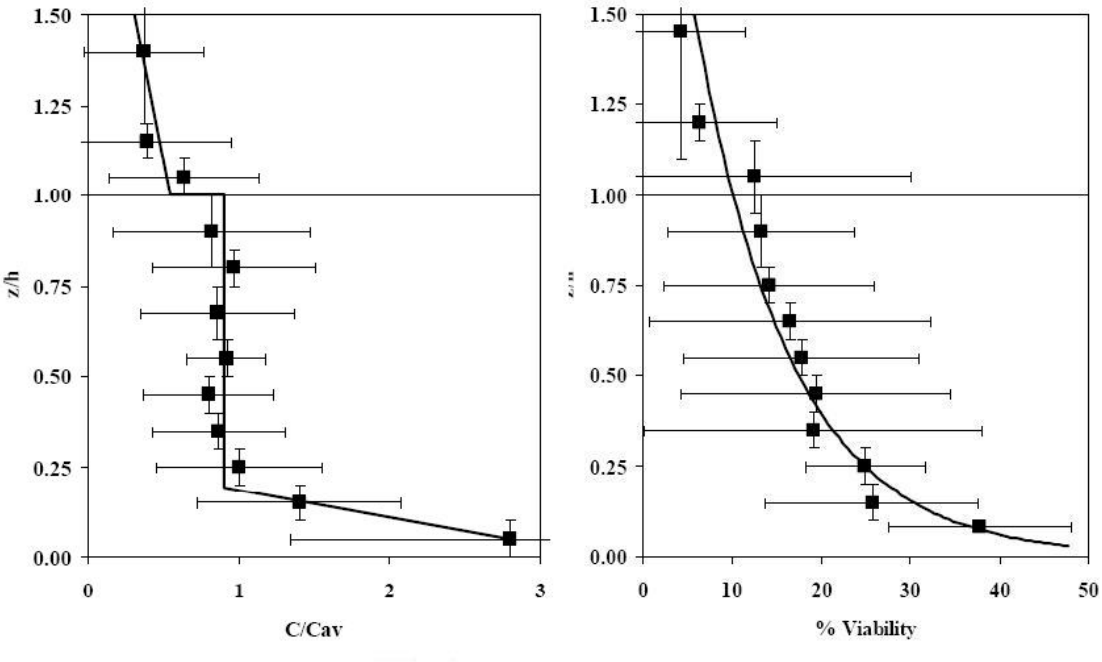

Figure 3.13 Vertical profiles of pollen concentration and viability (taken from Brunet et al 2001). The concentration profile has been normalized by the average concentration of pollen in the boundary layer. Height in both plots has been normalized by the height of the boundary layer top.

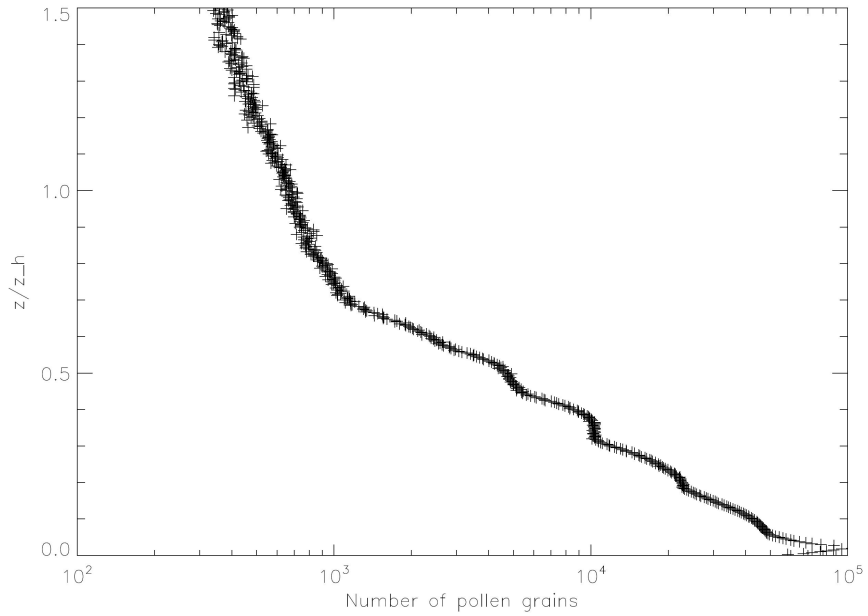
1.5
1.0
0.5
0.0
z/z_h
10^2
10^3
10^4
10^5
Number of pollen grains

(a)

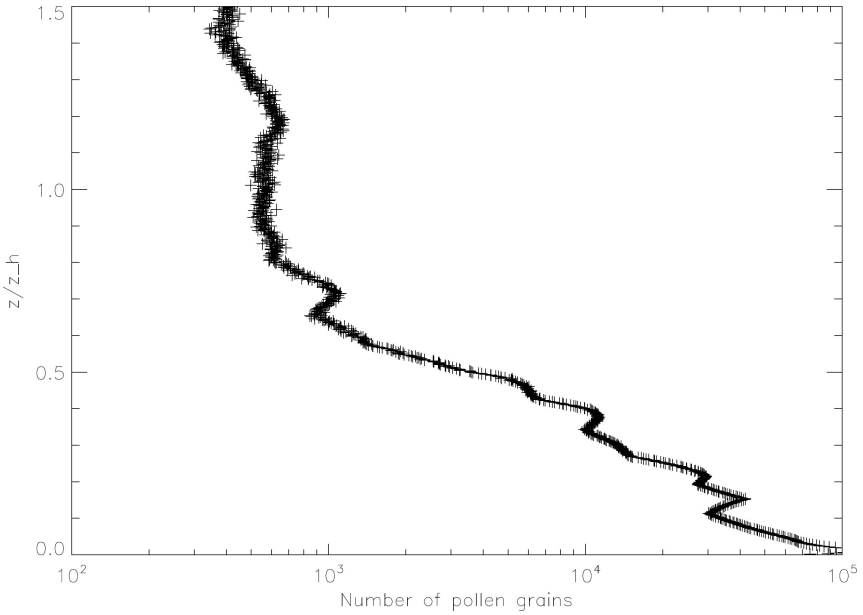
1.5
1.0
0.5
0.0
z/z_h
10^2
10^3
10^4
10^5
Number of pollen grains

(b)

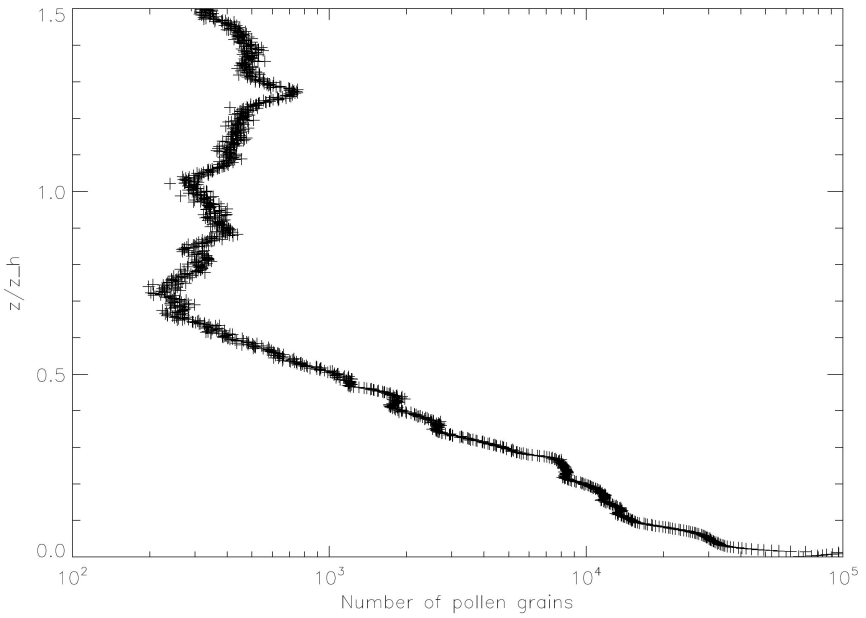

(c)

Figure 3.14 Vertical profiles of pollen concentration for 10:00 LST (a), 12:00 LST (b), and 14:00 LST (c). z_h is the height of the boundary layer top.

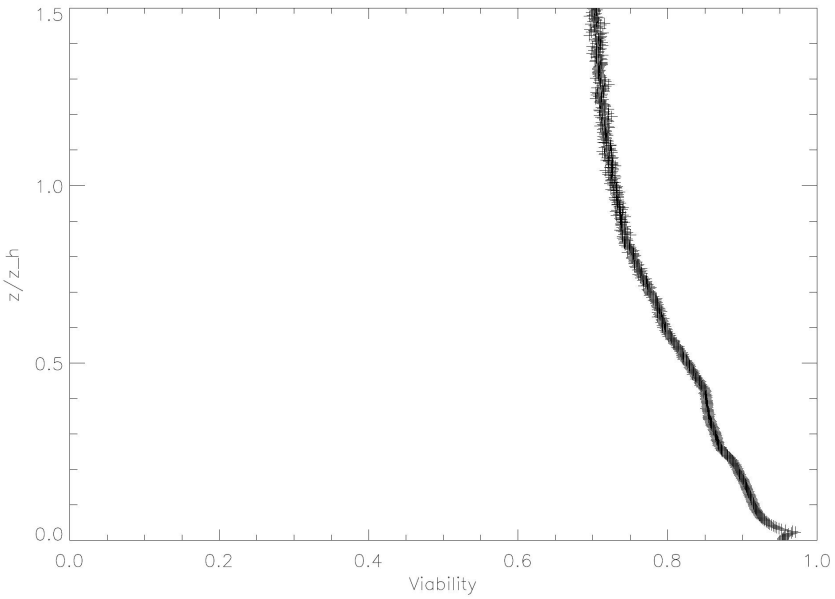
1.5
1.0
0.5
0.0
z/z_h
0.0
0.2
0.4
0.6
0.8
1.0
Viability

(a)

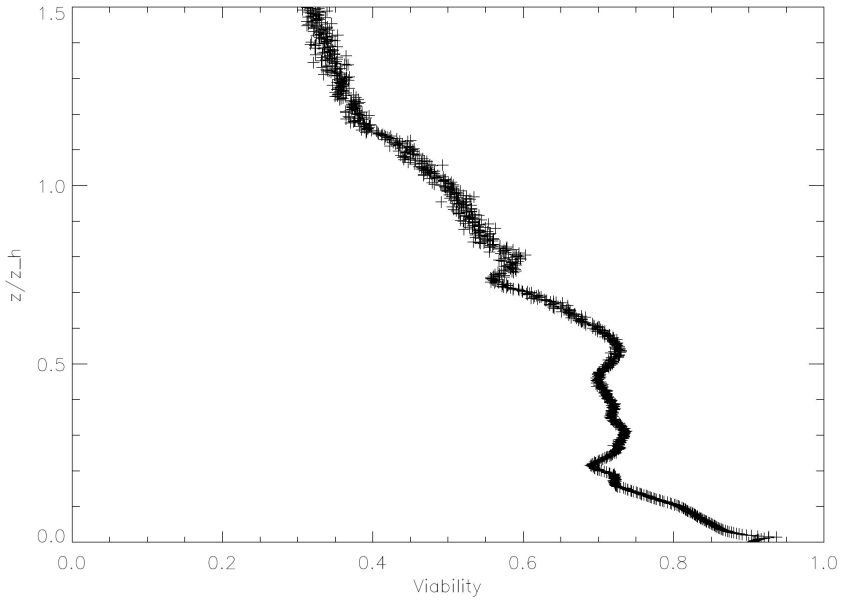
1.5
1.0
0.5
0.0
z/z_h
0.0
0.2
0.4
0.6
0.8
1.0
Viability

(b)

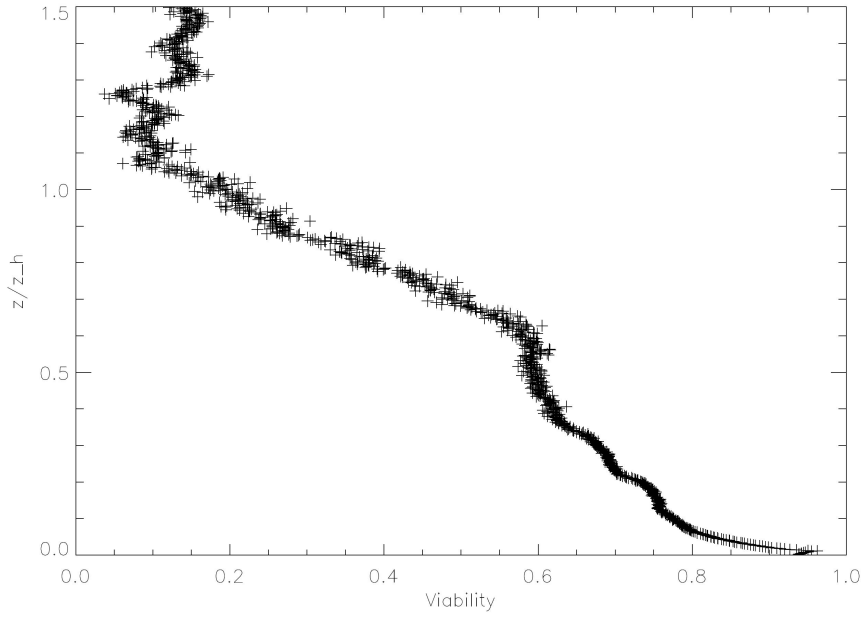

(c)

Figure 3.15 Vertical profiles of pollen viability for 10:00 LST (a), 12:00 LST (b), and 14:00 LST (c). z_h is the height of the boundary layer top.

CHAPTER 4. Conclusions

4.1 Summary and Discussion

With the increasing development of genetically modified crops, the need to quantify and control outcrossing between modified and conventional crops is becoming more important. A method for modeling the dispersion and viability of maize pollen was presented which combined the Advanced Regional Prediction System (ARPS), a Large-Eddy Simulation (LES) model, with a Lagrangian dispersion model (LDM).

The LES model was tested to ensure that its results were consistent with known behavior in the atmospheric boundary layer by creating profiles of vertical heat flux divergence at three different vertical grid spacings. Vertical heat flux divergence remained constant through the depth of the boundary layer, which implied that the rate of heating was constant through the layer. It was also observed to decrease through the day, which was attributed to an increasing depth of the boundary layer and a decreasing amount of energy being used to heat the layer, both of which have been observed in nature.

The development of the boundary layer was also examined by reporting the height of the boundary layer at points during the day. Since advection was treated within ARPS using a 4th-order equation in the horizontal and a 2nd-order equation in the vertical, the ideal vertical grid spacing was concluded to be half of the horizontal spacing. A lower or higher grid spacing ration exhibited generally realistic boundary layer growth, but may have suffered from anisotropy.

After testing, ARPS was used to simulate four days from a 2003 field study. Output fields of wind, temperature and humidity were read in by the LDM. This new version of the LDM was compared to a previous version which used a single sounding as input, and to field observations. This new version of the LDM tended to overpredict deposition within the first two hundred meters, but did deposit the majority of released pollen within this distance. Despite the maximum deposition occurring within a few hundred meters of the source, pollen was observed to travel over five kilometers in small concentrations.

Vertical profiles of pollen concentration and viability were compared to a second field study. While viable pollen was observed throughout the boundary layer, values of percent viability were much higher

than reported by Brunet et al (2001), while pollen concentration dropped off much faster with height than observed. It is possible that the results by Brunet et al may have included pollen advected from outside the study area which would have been older and less viable than pollen released from the study area. This process is not currently represented in the LDM.

The most significant finding of this research was the presence of viable pollen being transported over five kilometers, with the potential to be transported nearly twice that distance. While the chances of pollen outcompeting the pollen produced locally at a receptor field are small, it may be impossible to effectively impose isolation distances that would eliminate any chance of outcross. The distance that viable pollen travels was shown to be essentially a linear function dependent on the rate of water loss and wind speed. It may be possible to create simple mathematical models that would be able to reasonably predict the maximum distance of pollen transport based on simple measurements of wind, temperature and humidity.

4.2 Future Work

There are a number of improvements that can be added to the ARPS/LDM model to improve its accuracy:

1.) Increase the number of particles released,

2.) include canopy effects on the modeled wind structures in ARPS,

3.) integrating the LDM into ARPS so that updates to the wind fields can be received by the LDM instantaneously.

Being able to increase the number of particles being released would provide a much better overall prediction of pollen dispersion. One of the assumptions that was made in this study was that some amount of pollen would be lifted to the level where pollen was released. While this is not necessarily a bad assumption, it did result in underprediction of pollen deposition at the field edges. One of the limitations on modeling pollen dispersion is the availability of memory and computing power required to release larger amounts of particles. This limitation will be reduced over time as faster computers with more available memory are produced.

The inclusion of canopy effects on the wind would generate turbulence profiles that more closely reflect near surface observations. It has been observed that eddy diffusivity is enhanced above a crop canopy, which would have a significant impact on pollen transport (Mahrt 2000). Wind speeds are often observed to be reduced in and around maize canopies, so this would also increase the amount of pollen deposition near the source field.

The final improvement of running the LDM within the ARPS model would not likely have an impact on the results of the data. The benefits of this improvement would be increasing the efficiency of the running simulations compared to running ARPS and the LDM separately. A fair amount of time would be eliminated in writing output files from ARPS and reading them into the LDM. This would also drastically reduce the amount of physical memory required to store output files from both models.

4.3 References

Aylor, D. E., 1975: Deposition of particles in a plant canopy. *J. Applied Meteor.*, **14**, 52-57.

Mahrt, L., 2000: Surface heterogeneity and vertical structure of the boundary layer. *Bound.-Layer Meteorol.*, **96**, 33-62.